Systematic Entomology

Systematic Entomology (2020), DOI: 10.1111/syen.12463

Phylogenomic species delimitation in the ants of the *Temnothorax salvini* group (Hymenoptera: Formicidae): an integrative approach

MATTHEW M. PREBUS[1,2]

[1]School of Life Sciences, Arizona State University, Tempe, Arizona, U.S.A. and [2]Department of Entomology & Nematology, University of California, Davis, California, U.S.A.

Abstract. The members of the *Temnothorax salvini* (Forel) species group are rarely collected, arboreally nesting ants of Central American forests. Previously thought to consist of two broadly dispersed species, recent collections have revealed a diversity of specimens that defy the two-species *salvini* group concept, but these are difficult to distinguish from each other based solely on morphology. I contrast several model-based approaches to species delimitation based on target-enriched genomic data. With molecular data from thousands of ultraconserved elements (UCEs), mitochondrial genome sequences and morphometric data, I use an integrated approach to species delimitation within the *salvini* group. Morphometric data were analysed using cluster analysis of principal component analysis (PCA) output. I use several popular methods of molecular species delimitation, including bPTP, BPP and STACEY, using a novel approach to filtering UCE data based on posterior predictive checks of nucleotide substitution model adequacy. In addition, I use iBPP to integrate morphometric PCA data and filtered UCE data in a 'total evidence' analysis. I use geographical range data for an independent contrast to discriminate among competing species delimitation hypotheses. Furthermore, I investigate the evolutionary timescale and biogeographical history of the group and find that it arose roughly 13 Ma ago in habitats associated with present day mid-to-high elevations of the mountain complex spanning southern Mexico to northern Nicaragua. In addition, dispersal of the *salvini* group into the Southern Sierra Madre in Mexico, lowland habitats and the southern Central American cordilleras in Costa Rica and Panama subsequent to mountain building in southern Central America 5–8 Ma ago appears to follow a taxon-cycle dynamic, with the lowland-adapted *T. aztecus* representing the most recent expansion phase. I find that the *salvini* group, which previously contained two named species, is composed of nine, all of which are morphologically diagnosable *a posteriori*.

INTRODUCTION

Overview

Because species are the basic units of our planet's sexually reproducing biodiversity, it follows that our understanding of what constitutes species has broad implications in the biological sciences, including comparative biology (Tirosh *et al.*, 2007), conservation initiatives (Adams *et al.*, 2014; Fennessy *et al.*, 2016; Bercovitch *et al.*, 2017) and how the process of speciation occurs (Burbrink *et al.*, 2011; Domingos *et al.*, 2014; Barraclough, 2019).

In comparison to Sanger sequencing, advances in sequencing technology have provided several orders of magnitude more data to address a multitude of biological questions (Baird *et al.*, 2008; Bi *et al.*, 2012; Faircloth *et al.*, 2012; Lemmon *et al.*, 2012), yet the computational burden of analysing this wealth of information is out-of-step with many contemporary molecular species delimitation methods, especially those based on the multispecies

Correspondence: Matthew M. Prebus, School of Life Sciences, Arizona State University, P.O. Box 874501, Tempe, AZ 85287-4501. E-mail: mprebus@gmail.com

coalescent model (Takahata *et al.*, 1995; Rannala & Yang, 2003). Recent approaches to this issue have employed various data filtering approaches as a remedy to the computation-time/dataset size tradeoff, often using phylogenetic informativeness of whole loci as a guide (Andermann *et al.*, 2019; Pie *et al.*, 2019).

Along with the rise in data volume, the number of species delimitation approaches has burgeoned in recent years, so much so that Carstens *et al.* (2013) advocated for comparing the results of multiple methods in single studies in an effort to form a consensus. Often, the result of this approach has yielded large variations in the number of species delimited among methods. In order to discriminate between molecular species delimitation hypotheses, researchers typically require independent contrasts in the form of ecological, geographical or morphological data (Leaché & Fujita, 2010; Bauer *et al.*, 2011; Sistrom *et al.*, 2013; Masonick and Weirauch, 2020). While there have been a number of studies in arthropods, and the Formicidae specifically that have employed genomic data to aid species delimitation efforts (Ješovnik *et al.*, 2017; Longino & Branstetter, 2020), a small but growing number are using model-based and machine-learning approaches to species delimitation (Fujisawa *et al.*, 2016; Branstetter & Longino, 2019; Derkarabetian *et al.*, 2019; Gueuning *et al.*, 2020). In this study, I use target-enriched genomic data and contrast several popular model-based methods to construct species delimitation hypotheses in a group of closely related ant species.

The focal taxa of this study are the members of the *Temnothorax salvini* (Forel) species group (Prebus, 2017). The *Temnothorax salvini* group is defined as containing two species that have been previously described, *T. salvini* and *T. aztecus* (Wheeler), and their close, undescribed relatives. The *Temnothorax salvini* group is easily distinguished from its Central American congeners by the following diagnosis (this study): antennae consisting of 12 antennomeres; dorsal surfaces of legs and nearly all other surfaces of the body covered in long, tapering, suberect to subdecumbent setae; propodeum not strongly depressed (compare to *T. pergandei* Emery); metanotal groove often obscure; promesonotum grading evenly into propodeum, not bulging (compare to *T. pergandei*); dorsum of head above compound eyes and dorsum of mesosoma sculptured (compare to *T. politus* Smith). The members of the *Temnothorax salvini* species group are found throughout mainland Central America, typically nesting in dead twigs, hollow vines or under the roots of epiphytes in low elevation rainforest to high elevation cloud forest habitats. All nest collections thus far have contained a single dealate queen; it is likely that the members of this group, like many others in the *T. salvini* clade (*sensu* Prebus, 2017), are strictly monogynous. *Temnothorax salvini* and *T. aztecus* are remarkably similar in terms of morphology but can be readily separated by the colour of their integument (Baroni Urbani, 1978).

In the following, I use the terms '*salvini* clade', '*salvini* group' and '*salvini* complex'. For clarification, the *salvini* clade refers to a large group of heterogeneous species spanning North America to northern South America (Prebus, 2017); the *salvini* group is nested within the *salvini* clade and consists of similar appearing Central American species (Prebus, 2017, this study); the *salvini* complex is a group of closely related species found in the Central American Nucleus and the mountains of Costa Rica and Panama, which are difficult to distinguish based on morphology alone (this study).

The aims of this study are to investigate the phylogenetic relationships among the *salvini* group taxa and to establish species boundaries using an integrative taxonomic approach. The working hypothesis at the outset of this study was that *Temnothorax aztecus* and *T. salvini* represented colour variants of a widespread and morphologically variable species, similar to *T. pergandei* and *T. schaumii* (Roger) in eastern North America (Creighton, 1950; MacKay, 1993). However, preliminary phylogenetic analysis revealed that integument colour is stable across monophyletic groups, which occur in sympatry within the *salvini* species group, suggesting that colour is fixed within species and that what appear to be colour variants are different species.

This study is the product of four primary steps, which are elaborated upon in the following paragraphs: (1) generation of species delimitation hypotheses based on discovery methods with molecular data, (2) validation of the molecular species delimitation hypotheses using morphometric data, (3) validation of the molecular species delimitation hypotheses using a combined molecular and morphometric dataset and (4) estimation of the evolutionary timescale and biogeographic history of the *Temnothorax salvini* clade.

First, I employ a novel filtering strategy based on the extraction of coding nuclear sequence data from UCE reads, then use posterior predictive checks (Bollback, 2002) to extract codon positions that are readily modelled under one of the most universally used substitution models in molecular phylogenetics, the General Time Reversible model with gamma-distributed rate variation among sites (GTR+G). In addition, I assembled complete or nearly complete mitochondrial genomes from off-target UCE reads. I formed molecular species delimitation hypotheses (molecular operational taxonomic units, or MOTUs) by subsequently analysing these data under multiple species delimitation approaches in a manner advocated by Carstens *et al.* (2013).

Second, I use morphometric data from worker specimens of the *salvini* group to discriminate among and validate the MOTUs generated by the molecular approaches above by inputting these into a principal component analysis (PCA) and analysing the resulting output in maximum-likelihood cluster analyses.

Third, I used a combined molecular and morphological dataset to further clarify species boundaries in an integrative approach. The results of the morphometry PCA and filtered protein-coding UCE data were used as input for analysis using iBPP (Solís-Lemus *et al.*, 2015). In addition, I validated the integrated species delimitation hypotheses in the context of current MOTU distributions and Central American geography in an effort to discriminate between valid species and regional intraspecific morphological variation.

Finally, I use geographic range data and the consensus species delimitation hypothesis generated by the steps above to estimate the evolutionary timescale and the biogeographical history of the *Temnothorax salvini* group.

Table 1. Summary of datasets and analyses used in this study

Dataset	Programme	Analysis	Results
full_data	PartitionFinder2	Partitioning of UCE data	Additional Table 5
	IQ-TREE2	ML phylogeny of UCE data	Figure 1a
	ExaBayes	BI phylogeny of UCE data	Figure 1a
exon_data	PartitionFinder2	partitioning of protein coding UCE data	Additional Table 5
	IQ-TREE2	ML phylogeny of protein coding UCE data	Figure 1a
	ExaBayes	BI phylogeny of protein coding UCE data	Figure 1a
	bPTP	bPTP nuc species delimitation	Figure 2a
mt_data	PartitionFinder2	partitioning of mitochondrial gene data	Additional Table 6
	IQ-TREE2	ML phylogeny of mitochondrial gene data	Figure 1a
	ExaBayes	BI phylogeny of mitochondrial gene data	Figure 1a
	bPTP	bPTP mit species delimitation	Figure 2a
filtered_data	STACEY	STACEY nuc species delimitation	Figure 2a
	BPP	BPP nuc species delimitation	Figure 2a
	BEAST2	divergence dating	Figure 2b
	BioGeoBEARS	historical biogeography	Figure 4
filtered_data_&_mt_data	STACEY	STACEY nuc + mit species delimitation	Figure 2a
	BPP	BPP nuc + mit species delimitation	Figure 2a
morphology	Mclust	species delimitation validation	Figure 2a
	iBPP	iBPP morphology species delimitation	Figure 2a
filtered_data_&_mt_data_morphology	iBPP	iBPP all species delimitation	Figure 2a

Material and methods

See Table 1 for an overview of the datasets and the associated analyses used in this study.

Taxon sampling. A total of 112 workers of the *salvini* group, including individuals from 67 nests and 40 populations, were selected to represent the geographic range and morphological variability of the group. Twenty five specimens were used for molecular analysis, and five outgroup species from the more inclusive *salvini* clade were selected to root the initial phylogenetic tree but were excluded from downstream analyses. Voucher specimens used for DNA extractions in this study are deposited at the University of California, Davis Bohart Museum of Entomology collection (UCDC). Specimens used for morphometric analyses are deposited in the California Academy of Sciences Entomology Collection (CASC), the personal collection of John Longino at the University of Utah (JTLC), the Natural History Museum of Los Angeles Entomology Collection (LACM), the collection of the author (MMPC) and UCDC. Unique specimen identifiers and collection data can be found in Supplementary Table S1 and at AntWeb (http://antweb.org).

Ultraconserved elements sequence generation. DNA was extracted nondestructively from adult worker ants using a DNeasy Blood and Tissue Kit (Qiagen, Inc.) following the manufacturer's protocols. I input up to 50 ng of DNA, sheared to a target fragment size of 400–600 bp into a genomic DNA library preparation protocol for targeted enrichment of ultranconserved elements (UCEs) following Faircloth *et al.* (2015) as modified by Branstetter *et al.* (2017) using a unique combination of iTru barcoding adapters for each sample. I performed enrichments on pooled libraries using the custom version of the Hym 2.5 Kv 2A ant-specific RNA probes (Branstetter *et al.*, 2017; Arbor Biosciences, Ann Arbor, MI), which target 2524 UCE loci in the Formicidae. I followed the library enrichment procedures for the probe kit, except that I reduced the RNA probe concentration to 0.1X (note that this step is only necessary for the custom kit; the currently available catalogue kit is already diluted to 0.1X concentration), used custom adapter blockers instead of the standard blockers, and left enriched DNA bound to the streptavidin beads during PCR, as described in Faircloth *et al.* (2015). Following post-enrichment PCR, I purified the resulting pools using Speed-Bead magnetic carboxylate beads (Rohland & Reich, 2012; Sigma-Aldrich) and adjusted their volume to 22 μL.

I verified enrichment success and measured size adjusted DNA concentrations of each pool with qPCR using a SYBR® FAST qPCR kit (Kapa Biosystems) and a Bio-Rad CFX96 RT-PCR thermal cycler (Bio-Rad Laboratories) and combined all pools into an equimolar final pool. The final pool was sequenced as a single lane at the High Throughput Genomics Facility at the University of Utah on an Illumina HiSeq 2500 (125 cycle paired end sequencing v4).

Sequence processing and phylogenetic inference: UCEs. Because this study involves reducing the full UCE dataset to a size that accommodates computational limitations, I generated several successively smaller datasets and analysed them to ensure that there were not any major conflicts in topology or statistical support between the resulting trees. Below, I describe the production of three datasets: the first consists of the full set of UCE loci from the *salvini* group specimens and outgroups; the second is protein coding data extracted from the full UCE dataset; the third is a dataset consisting phased, protein coding data from the *salvini* group specimens, without outgroups.

While the precise nature of what UCEs are composed of in the ant-specific probe set is still uncertain, they are most likely a combination of exon and intron sequence data similar to other sets of UCEs (McCole *et al.*, 2018). In fact, previous studies have successfully extracted exon sequence from large UCE datasets (Prebus, 2017; Borowiec, 2019). Intron sequence has numerous well documented issues with structure-linked sequence evolution (Learn *et al.*, 1992; Clegg *et al.*, 1994; Kelchner, 2002; Haddrill *et al.*, 2005), and heterogeneous evolutionary rates both within introns and between introns and their abutting exons (Hughes & Yeager, 1997; Kelchner, 2002; Subramanian & Kumar, 2003). While it is certain that intron sequence contains information that is useful for phylogenetic reconstruction, the matter of how to address the evolution of intron sequence, and whether it has significant downstream effects on phylogenetic analysis of genomic datasets remains uncertain. In this study, I conservatively chose to focus on exon sequence data extracted from UCEs, which often have predictably different rates of evolution between codon positions due to codon redundancy and the conservation of amino acids. These codon positions can then be input as datablocks into partitioning analysis for the larger dataset or used as natural partitions in gene tree analyses. In addition, I decided to use phased UCE data in the species delimitation analyses because it has been demonstrated to yield more accurate species delimitation hypotheses based on data simulations (Andermann *et al.*, 2019), and because analyses of these data have an inherent threshold for species limits. For example, analyses that delimit phased locus data from a single specimen into two species are over-splitting and should be rejected.

Following sequencing, raw reads were trimmed of adapter contamination, Illumina sequencing artefacts and low-quality bases using *illumiprocessor*, which is included in PHYLUCE v1.6.6 (Faircloth, 2016). Cleaned reads were assembled denovo with PHYLUCE using Trinity v2.1.1 (Grabherr *et al.*, 2011). All newly generated raw sequence reads have been submitted to the National Center for Biotechnology Information (NCBI) Sequence Reads Archive (BioProject PRJNA669896; see Supplementary Table S3).

Generation and phylogenetic analysis of the 'full_data' dataset. I followed the standard PHYLUCE protocol for processing UCEs in preparation for phylogenomic analysis, aligning the monolithic unaligned fasta file with the phyluce_align_seqcap_align command, using MAFFT (Katoh & Standley, 2013) as the aligner (-aligner mafft) and opting not to edge-trim the alignment (-no-trim). I trimmed the resulting alignments with the phyluce_align_get_gblocks_trimmed_alignments_from_untrimmed command in PHYLUCE, which uses GBlocks v0.91b (Castresana, 2000), using the following settings: b1 0.5, b2 0.5, b3 12, b4 7. After removing UCE locus information from taxon labels using the command phyluce_align_remove_locus_name_from_nexus_lines, I examined the alignment statistics using the command phyluce_align_get_align_summary_data, and generated a dataset in which each locus contains a minimum of 90% of all taxa using the command phyluce_align_get_only_loci_with_min_taxa. I used the command phyluce_align_format_nexus_files_for_raxml to concatenate these loci into a single alignment and generate a partition file to use as input for the SWSC-EN method (Tagliocollo & Lanfear, 2018). The resulting matrix is referred to as the 'full_data' dataset below. The resulting datablocks were used as input for PartitionFinder2 (Lanfear *et al.*, 2016). I used the best partitioning scheme as input for Exabayes 1.5 (Aberer *et al.*, 2014), using GTR+G as a substitution model. I ran two independent analyses (numruns 2) for 10 M generations per run, sampling every 500 generations. Because initial runs of this analysis yielded unrealistically long trees, I followed the advice of Brown *et al.* (2010) and calculated lambda for an informative exponential prior on branch lengths (brlenPr) with a custom script written in R (exabayes_lambda_calculation.R; see Dryad repository accompanying this article) using the starting tree generated by RAxML (Stamatakis 2014) for the PartitionFinder2 analysis as input. I assessed convergence and burn-in proportion using Tracer to analyse log files, and combined the tree files with a burn-in of 10%, reducing sampling frequency to every 5 K generations, for a combined tree file containing 3600 trees. Finally, I used 'consense' to generate a consensus tree. I also used the partitioned dataset as input for tree inference in IQ-TREE 2.0.8 (Nguyen *et al.*, 2015), using 1000 ultrafast bootstrap replicates (-bb 1000).

Generation and phylogenetic analysis of the 'exon_data' dataset. I split the monolithic unaligned fasta file into individual loci using the PHYLUCE command phyluce_assembly_explode_get_fastas_file, removed the locus identifiers from the taxon names in each locus file with the command-line tool 'sed', and used these files as input for the pipeline uce_to_protein.py (Borowiec, 2019). RNA-Seq reads of *Temnothorax curvispinosus* (Mayr) were downloaded from NCBI (BioProject PRJNA450816) and were used as a query reference. The amino acid translations for each locus output by the pipeline was aligned using MAFFT, and these alignments were then used as a reference to realign the extracted nucleotide data using the local version of TranslatorX (Abascal *et al.*, 2010). The aligned loci were then trimmed using phyluce_align_get_gblocks_trimmed_alignments_from_untrimmed. I inspected each locus alignment by eye using Aliview (Larsson, 2014) and discarded sequences that were mismatched and most likely contaminants. I used AMAS (Borowiec, 2016) to calculate number of taxa and matrix length for each protein-coding locus, and concatenated loci that had ≥90% taxon presence and were ≥150 bp long into a single matrix. This dataset is referred to below as 'exon_data'. I partitioned this alignment into datablocks by locus and codon position (positions 1+2 and 3) and used these as input into PartitionFinder2, using the Bayesian Information Criterion (BIC) as the search criterion and limiting the models considered to GTR+G. I used the rcluster search algorithm (Lanfear et al. 2014), limiting the maximum number of similar subsets considered to the top 500 and the percentage of subsets considered to the top 5% (-rcluster-max 500, -rcluster-percent 5) to reduce computation time. I analysed the partitioned

dataset with ExaBayes (Aberer *et al.*, 2014), calculating a prior on branch lengths as above, using GTR+G, four independent analyses (numruns 4), four coupled chains (numCoupledChains 4) and four swaps per generation (numswapspergen 4) for 10 M generations per analysis, sampling every 1 K generations. I assessed convergence and burn-in proportion using Tracer, and combined output tree files with a burn-in of 10%, reduced sampling frequency to every 4 K generations for a combined tree file containing 9991 trees. Finally, I used 'consense' to generate a consensus tree. I also used the partitioned dataset as input for model selection and tree inference in IQ-TREE2, using the -MFP option to select models for the partition scheme output by PartitionFinder2, followed by bootstrap analysis using 1000 ultrafast bootstrap replicates (-bb 1000).

Generation of the 'filtered_data' dataset. I aligned the monolithic fasta file using the command phyluce_align_seqcap_align and MAFFT, but permitted locus edge-trimming following alignment. The aligned, trimmed loci were then split into separate fasta files using phyluce_align_explode_alignmentswith the '-by-taxon' option. The exploded alignments were allele-phased using the protocol developed by Andermann *et al.* (2019). Essentially, the phasing pipeline involves mapping the illumiprocessor cleaned reads onto UCE loci using the PHYLUCE command phyluce_snp_bwa_multiple_align, which uses the Burrows-Wheeler Alignment algorithm bwa-mem (Li, 2013), and subsequently allele-phasing the mapped reads using the command phyluce_snp_phase_uces. The monolithic, unaligned fasta file of allele-phased UCE loci was then split into individual loci using phyluce_assembly_explode_get_fastas_file and the sample names were cleaned of locus data using the command line tool 'sed'. The phased data were input into the uce_to_protein pipeline and aligned as above for the 'exon_data' dataset. In the following, posterior predictive checks are implemented as a filtering mechanism. Because the complexity of the General Time Reversible (GTR) nucleotide substitution model usually accommodates the substitution rates and occurrence frequencies observed in large alignments, many phylogenetic analysis programmes use a version of it as a default. While GTR+G is usually the best fitting nucleotide substitution model for large datasets, the adequacy of this substitution model is often taken for granted. The steps in posterior predictive checks address model adequacy by first analysing empirical data in a Bayesian framework, then using the posterior distributions of parameters generated by the analysis of the empirical data to simulate data multiple times, and then a test statistic is calculated for the empirical data and the simulated datasets. If the value calculated for the test statistic of the empirical data falls within the distribution of the calculated values of the simulated data, model adequacy is supported. I wrote a custom script in RevBayes (Höhna *et al.*, 2016; see Dryad repository accompanying this article) to partition each protein coding locus by codon position (positions 1+2 and 3) and to perform posterior predictive checks on each partition using GTR+G as a substitution model and multinomial likelihood as a test statistic, which is indicative of the overall model fit. I assessed model adequacy using a two tailed t-test and size effect as criteria, then ranked each partition, which included all 25 ingroup taxa: first by p-value, then by size effect and selected the 50 best data partitions, referred to below as 'filtered_data'.

Generation and phylogenetic analysis of the 'mt_data' dataset. Because mitochondrial sequences often have large repetitive regions that can complicate assembly, I followed the advice of the NOVOplasty tutorial (Dierckxsens *et al.*, 2016) and used *trimmomatic* 0.38 (Bolger, 2014) to trim adapter contamination and Illumina sequencing artefacts from the raw UCE reads, without additional quality trimming. For each set of raw reads, I used the associated adapter fasta file generated by initial processing with illumiprocessor (ILLUMINACLIP:adapters.fasta:2:30:10), and omitted the LEADING, TRAILING and SLIDINGWINDOW options that are used by default in *illumiprocessor*. I used these adapter-cleaned reads as input for the programme mitoFinder (Allio *et al.*, 2020) using the mitogenome of *Vollenhovia emeryi* (NCBI BioProject PRJNA278668) as a reference and MetaSpades (Nurk *et al.*, 2017) for assembly. I used the longest contig output from mitoFinder as input for mitoBim (Hahn *et al.*, 2013) to extend the contig and to assess coverage depth, as viewed in Tablet (Milne *et al.*, 2013). In cases where mitoFinder did not assemble the full mitogenome, I used the mitogenome of the closest related specimen, as determined from the UCE phylogenetic inference above, as a reference backbone for assembly with mitoBim. The final assemblies were annotated automatically via the MITOs webserver (Bernt *et al.*, 2013). Full mitochondrial genome sequences were deposited at GenBank (accession numbers MW233593–MW233617; see Supplementary Table S3).

DNA sequence data for mitochondrial protein coding genes were extracted using the annotation results and aligned with MAFFT; this dataset is referred to here as 'mt_data'. Each of the 13 genes was partitioned by codon position (position 1+2 and 3). For Bayesian inference (BI), I used PartitionFinder2 to partition data with the substitution models used by MrBayes. I excluded models invoking both gamma distributed among-site rate variation and proportion of invariable sites (i.e., +I+G) due to the interactions of these parameters that may cause anomalies (Sullivan & Swofford, 2001; Yang, 2006). Following model selection and partitioning, I used MrBayes v3.2.6 (Huelsenbeck & Ronquist, 2001; Ronquist & Huelsenbeck, 2003) to infer the mitochondrial phylogeny, using two runs with four chains each, sampling every 2500 generations for a total of 25 M generations. I inspected convergence using Tracer and used the default 25% burn-in when summarizing the two runs. Similarly, I used the data blocks from above as input for partitioning and model testing in IQ-TREE2. I edited the input partition nexus file to exclude +I+G combinations and used the −MFP+MERGE (Kalyaanamoorthy *et al.*, 2017) command. I employed 1000 ultrafast bootstrap replicates (-bb 1000) (Hoang *et al.*, 2018).

Molecular species delimitation. The programme bPTP (Zhang *et al.*, 2013), which is a Bayesian implementation of

the Poisson Tree Process species delimitation method, was used to generate a first set of species delimitation hypotheses. I used the posterior distribution of trees from BI analysis of the 'exon_data' dataset as input for the local version of bPTP. I removed outgroups and used 100 K Markov chain Monte Carlo (MCMC) iterations, leaving all other parameters at default values (sampling every 100 generations, with a burn-in of 10%). I also used the BI posterior distribution of the 'mt_data' dataset as input for bPTP using the parameters above.

For the following two analyses, I used two datasets: the 'filtered_data' dataset and the 'filtered_data_&_mt_data' dataset, which is a combination of the 'filtered_data' and 'mt_data' datasets. Both were used as input for STACEY (Jones, 2017) as implemented in BEAST2 (Bouckaert *et al.*, 2019). STACEY uses the multispecies coalescent (MSC) model to infer a "species or minimal clusters" (SMC) tree under the birth-death-collapse tree prior, without no requirement of a guide tree. The programme BEAUti, using the STACEY template, was used to generate the input files for BEAST2. For the analysis of 'filtered_data_&_mt_data', all mitochondrial gene trees were linked, assuming no mitochondrial recombination; also, phased UCE partitions and mitochondrial alignments were assigned to one species/population representing each sample in the 'Taxon sets' pane. For both datasets, nucleotide substitution models for each partition were set to 'RB' with four gamma categories to account for rate heterogeneity. I set the bdc Growth Rate prior to a lognormal distribution with $M = 4.6$ and $S = 2.0$, clock Rate prior for each partition to lognormal and pop Prior Scale to lognormal, changing the default shape parameters to $M = -7.0$ and $S = 2.0$. Due to slow convergence in initial runs of the 'combined' dataset analysis, I imposed three monophyletic constraints on the SMC tree, fixing the topology of *Temnothorax salvini* grp 1, *T. salvini* grp 2, *T. salvini* grp 3 and *T. salvini* grp 4, all of which were recovered as monophyletic in phylogenetic analyses of the datasets above. I set the MCMC chain length to 2 billion generations, storing every 10 M, with two independent analyses for each dataset. The two runs of each treatment were combined via logcombiner, with a burn-in of 25%, and input into species Delimitation Analyser using default settings.

BPP (Yang, 2015) was also used for species delimitation for comparison with the previous two models. Similar to STACEY, the A10 analysis in BPP is also a Bayesian method that uses the MSC model but uses the more computationally intensive reversible-jump Markov chain Monte Carlo algorithm to calculate species delimitation probabilities on a fixed species tree. For all of the BPP and iBPP analyses that follow, I used the topology inferred from the BI analysis of the 'exon_data' dataset as a guide tree. I used the 'filtered_data' and 'filtered_data_&_mt_data' datasets as input. First, tau and theta parameters were estimated using the A00 analysis on a fixed tree from the BI analysis of the 'exon_data' dataset, without delimitation. Using the resulting parameters, I employed the rjMCMC species delimitation algorithm 1 (species delimitation = 1 1 2 1). Because mitochondrial sequence and nuclear data have heterogeneous mutation rates, I estimated locus rate using an alpha of five for the Dirichlet distribution (locusrate = 1 5). I set the number of MCMC generations to 200 K, sampling every five generations, with a 25% burn-in. I ran ten independent analyses for the two datasets, then averaged the posterior probabilities for presence of nodes across for each dataset. I considered nodes with 95% posterior probability or greater as strongly supported.

Morphological analysis. A total of 112 worker specimens from the *salvini* group, which included individuals from 67 nests, 40 populations and the 25 voucher specimens from the molecular analysis were selected for morphological clustering analysis. To generate the 'morphology' dataset, specimens were measured at a maximum magnification of ×63 using a Leica MZ12.5 stereomicroscope, a movable stage equipped with orthogonal digital micrometres, and an ocular graticule. The following is a list of measurements used in this study, many of which are based on Seifert & Csősz (2015) and Csősz & Fisher (2015). They are also depicted in Fig. 1.

SL	Scape length. Maximum scape length excluding the basal neck and the articular condyle (see Fig. 1a).
EL	Maximum diameter of the compound eye (see Fig. 1d).
EW	Minimum diameter of the compound eye (see Fig. 1d).
FRS	Frontal carina distance. Distance of the frontal carinae immediately caudal of the posterior intersection points between frontal carinae and torular lamellae. If these dorsal lamellae do not laterally surpass the frontal carinae, the deepest point of scape corner pits may be taken as the reference line. These pits take up the inner corner of the scape base when the scape is directed fully caudally and produces a dark, triangular shadow in the lateral frontal lobes immediately posterior to the dorsal lamellae of the scape joint capsule (see Fig. 1a).
HW	Maximum width of the head, including the compound eyes (see Fig. 1a).
HWb	Maximum width of head capsule without the compound eyes, measured posterior to the eyes (see Fig. 1a).
HL	Maximum cephalic length. The head must be carefully tilted to the position, providing the true maximum. If excavations of the posterior margin of the head capsule and/or anterior margin of the clypeus are present, then the measurement is@ taken from an imaginary line that spans the excavations from the posterior- or anterior-most margins (see Fig. 1a).
PoOC	Postocular distance. Adjust the head to the measuring position of CL. Using an ocular graticule, the length between posterior margin of the compound eyes and the posterior margin of the head capsule. If the posterior margin of the head capsule is excavated, then the measurement is taken from an imaginary line that spans the

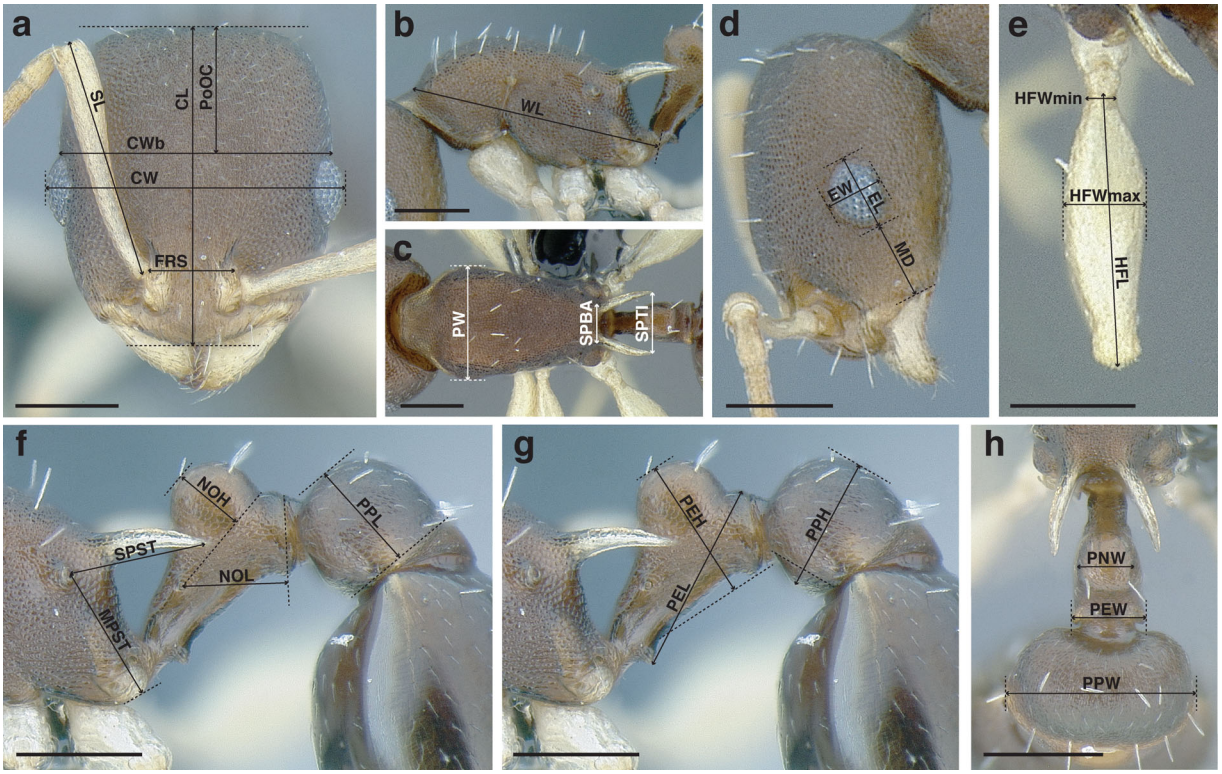

Fig 1. Measurements used in this study, using the worker of *Temnothorax albispinus* (Wheeler), CASENT0756097, as a model (a) head in full face view, (b) mesosoma in profile view, (c) mesosoma in dorsal view, (d) head in profile view, (e) metafemur in dorsal view, (f and g) propodeum and waist segments in profile view, (h) waist segments in dorsal view.. [Colour figure can be viewed at wileyonlinelibrary.com].

excavation from the posterior-most margins (see Fig. 1a).

MD Malar distance. Minimum Distance from the anterior margin of the compound eye to where the mandible articulates with the head capsule (see Fig. 1d).

WL Weber's length. Distance between the caudal most point of propodeal lobe to the inflection point between the pronotal neck and the pronotal declivity (see Fig. 1b).

SPST Propodeal spine length. Distance between the centre of the propodeal spiracle and tip of the propodeal spine (see Fig. 1f).

MPST Maximum distance from the centre of the propodeal spiracle to the posteroventral corner of the ventrolateral margin of the metapleuron (see Fig. 1f).

PEL Petiole length. Diagonal petiolar length in lateral view; measured from anterior corner of subpetiolar process to dorso-caudal corner of caudal cylinder (see Fig. 1g).

NOL Petiolar node length. Measured in lateral view from the centre of the petiolar spiracle to the dorso-caudal corner of caudal cylinder. Do not erroneously take as the reference point the dorso-caudal corner of the helcium, which is sometimes visible (see Fig. 1f).

NOH Petiolar node height. Maximum height of the petiolar node, measured in lateral view from the uppermost point of the petiolar node perpendicular to a reference line set from the petiolar spiracle to the imaginary midpoint of the transition between the dorso-caudal slope and dorsal profile of caudal cylinder of the petiole (see Fig. 1f).

PPL Postpetiole length. The longest distance, perpendicular to the posterior margin of the postpetiole, between the posterior postpetiolar margin and the anterior postpetiolar margin (see Fig. 1f).

PEH Petiole height. The longest distance measured from the ventral petiolar profile at node level (perpendicular to the chord length of the petiolar sternum) to the distal most point of the dorsal profile of the petiolar node (see Fig. 1g).

PPH Maximum height of the post petiole in lateral view measured perpendicularly to a line defined by the linear section of the segment border between postpetiolar tergite and sternite (see Fig. 1g).

PW	Pronotum width. Maximum width of the pronotum in dorsal view (see Fig. 1c).
SPBA	Minimum propodeal spine distance. The smallest distance of the lateral margins of the propodeal spines at their base. This should be measured in antero-dorsal view: the wider parts of the ventral propodeum do not interfere with the measurement in this position. If the lateral margins of propodeal spines diverge continuously from the tip to the base, a smallest distance at base is not defined. In this case, SPBA is measured at the level of the bottom of the interspinal meniscus (see Fig. 1c).
SPTI	Apical propodeal spine distance. The distance of propodeal spine tips in dorsal view; if spine tips are rounded or truncated, the centres of spine tips are taken as reference points (see Fig. 1c).
PNW	Maximum width of petiolar node in dorsal view (see Fig. 1h).
PEW	Maximum width of petiole in dorsal view, measured across the posteriormost margin (see Fig. 1h).
PPW	Postpetiole width. Maximum width of postpetiole in dorsal view (see Fig. 1h).
HFL	Hind femur length. Maximum length of the metafemur in dorsal view (see Fig. 1e).
HFWmax	Maximum metafemur width in dorsal view (see Fig. 1e).
HFWmin	Minimum metafemur width in dorsal view (see Fig. 1e).
HS	Absolute cephalic size. The arithmetic mean of HL and HWb.
ES	Absolute eye size. The arithmetic mean of EL and EW.

I used scripts modified from Baur & Leuenberger (2011) to perform a multivariate ratio analysis in R (R Core Team, 2019) on the full dataset, and six additional taxon subsets, which divided the full taxon set into groups by geographical area or into groups that are morphologically similar. I used the output of the principal component sub-analysis as input for maximum likelihood cluster analysis using *mclust* (Scrucca *et al.*, 2016) on each dataset. For each cluster analysis, I analysed two datasets: one consisting of the first two principal components (PCs) and the other consisting of the set of PCs that explained 75% of the variation. Vouchers and their nestmates were assigned to MOTUs based on the molecular analyses above, and error rate was calculated by the proportion of vouchers or their nestmates that were misclassified to MOTU. Among the two sub-analyses, the one with the lowest error rate was selected for presentation as morphological species delimitation hypotheses. A list of all specimens used in the morphological analysis, along with unique identifiers and collection data can be found in Supplementary Table S1.

Because the majority of clustering sub-analyses using PCs that explained 75% of the data variation had the lowest error rate, I used the first four PCs as input for a morphology-only analysis in iBPP (Solís-Lemus *et al.*, 2015). I set *the taprior* to 3, 200 and *tauprior* to 3, 100. I set the number of MCMC generations to 200 K, sampling every five generations, with a 25% burn-in. I ran ten independent analyses, then averaged posterior probabilities for presence of nodes across for each dataset. For this analysis, I considered nodes with simple majority rule as well supported.

Total evidence analysis. I used iBPP to perform a joint molecular and morphometric species delimitation analysis, using 'filtered_data_&_mt_data' molecular dataset and the first four PCs from the morphological analysis, referred to here as the 'filtered_data_&_mt_data_morphology' dataset. I configured the control file as above for the iBPP morphology-only analysis and ran ten independent analyses, averaging posterior probabilities for presence of nodes across for each dataset. For this analysis, I considered nodes with 95% posterior probability or greater as strongly supported.

Delimitation scheme decision. In the following, I endeavoured to use the biological species concept (Mayr, 1942) as a guiding principle for validation of species delimitation hypotheses, using molecular data, morphology and geographical range data as a proxy to determine whether the populations that my samples were taken from are reproductively isolated. Closely related samples (determined by phylogenetic analysis), which are morphologically divergent from each other (determined by morphological analysis) are critically examined within the context of the geographical range of the clade that contains them, with the default assumption that they are populations of morphological variants of the same species if they inhabit the extremes of the overall range of the clade.

I used the following rationale to discriminate among the species delimitation schemes generated by the analyses above: if the molecular and methods conflicted in how they delimited a given clade, they were contrasted with the results of the morphological delimitation analyses, and the least-split scheme shared between the molecular and morphology delimitation analyses was used. The delimitation schemes were then further evaluated in terms of geography, that is, whether sister taxa in the more finely delimited scheme were sympatric, that is, had range overlap (were collected in the same locality); if sister taxa were not sympatric, that is, a delimited taxon was at a geographical extreme of the overall range of the combined sister taxa, then they were considered divergent geographical variants of the same species and lumped accordingly.

Divergence dating analysis. I used BEAST2 v2.5.2 (Bouckaert *et al.*, 2019) to infer divergence dates using the 'filtered_data' sequence dataset as input. I linked clock models and trees across the partitions, used the reversible jump algorithm 'RB' to average over substitution models for each partition, used a four-category gamma distribution to estimate among site rate variation, and set the clock model to 'Relaxed Clock Log Normal'. I used a birth-death tree prior because it has been found that it leads to more accurate divergence estimates in simulated analyses, when dataset include inter- and intraspecific sampling

(Ritchie *et al.*, 2017). Because there were no fossils available for the taxon set used in this study, I set two secondary calibration points based on the chronogram estimated in Prebus (2017), which used a total evidence tip-dating approach to estimate the divergence dates of *Temnothorax* using Baltic and Dominican amber fossils to calibrate the analysis:

1 root: uniform distribution, lower 6.0 Ma ago, upper 29.0 Ma ago, encompassing the upper limit of the 95% highest posterior density (HPD) of the divergence date of the *salvini* group and its sister species and the lower limit of the divergence of the most recent common ancestor (MRCA) of *Temnothorax aztecus* and *T. salvini*
2 node subtending P048 + P050: normal distribution, sigma 3.0, offset 11.0 Ma ago, encompassing the 95% HPD of the divergence date of *Temnothorax aztecus* and *T. salvini*.

I set the number of generations to 100 M, logging every 10 K generations, and ran two independent analyses. I used Tracer to monitor chain mixing and convergence. Following completion, I combined the two runs using LogCombiner, discarding the default first 25% of each run and sampling every 20 K states for a total of 7500 trees. I used TreeAnnotator to annotate the final tree using default settings.

Historical biogeography. BioGeoBEARS (Matzke, 2013) was used to infer patterns of historical biogeography in the *salvini* group. I used the chronogram generated by the divergence dating analysis above and pruned the tree to tips representing nine species based on the results of the species delimitation decision above. I delimited the range of the *salvini* group into three regions based on major mountain ranges and mountain complexes in Central America: the southern Sierra Madre (SSM), a mountain range in southern Mexico, which extends from southern Michoacán state to the Isthmus of Tehuantepec in eastern Oaxaca state; the Central American Nucleus (CAN), composed of all mountain ranges between the Isthmus of Tehuantepec and the Nicaraguan depression; the southern Central American cordilleras (SCA), located between the Nicaraguan depression and the Isthmus of Panama (see Fig. 2). I further divided these three general areas by altitudinal zonation, considering low elevation to be <1000 m, mid elevation 1000–1800 m and high elevation >1800m. I altered the default BioGeoBEARS R script to include a time stratified analysis, taking into account mountain building in the SCA8-5 Ma ago (Duque-Caro, 1990; Kirby, 2007; Denyer & Kussmaul, 2012). I ran four analyses in which I contrasted scenarios with different dispersal probabilities and areas allowed at different time periods. Because the CAN and the SCA are hypothesized to have been separated by shallow marine waters during much of the Miocene (Iturralde-Vinent & MacPhee, 1999), the 'areas allowed' matrix was adjusted to disallow dispersal between the CAN and the SCAprior to 8 Ma ago for scenarios M2 and M3. For scenarios M1 and M2 the 'dispersal multipliers' matrix was set for moderately difficult dispersal (0.01) between these areas between 8 and 5 Ma ago following the findings of Bacon *et al.* (2015), which suggest that dispersal of land animals occurred between northern South America and southern Central America during this time period. For each scenario, I compared three dispersal models in BioGeoBEARS (DEC, DIVA-like and BayArea-like). I did not include models with the jump-dispersal parameter (+j) because it has been demonstrated that models including this parameter are not comparable to models without it in a statistical testing framework (Ree & Sanmartín, 2018).

Results

Sequence processing and phylogenetic inference: UCEs

Following assembly and UCE extraction, the mean number of UCE loci per specimen was 2309, with a mean contig length of 743 bp, and a mean coverage score of 46× (see Supplementary Table S2). Following alignment, trimming and filtering of the full UCE dataset to loci with ≥90% taxon presence, the 'full_data' dataset had 2077 loci, with a mean locus alignment length of 690 bp. The concatenated matrix was 1 452 209 bp in length, in which 162 000 sites (11.2%) were variable, 47 401 sites (3.3%) were parsimony informative, with 11.2% missing data. After extracting protein coding loci and filtering the dataset to loci with ≥90% taxon presence and ≥150 bp, the 'exon_data' dataset had 686 loci, with a mean locus alignment length of 373 bp. The concatenated matrix was 256 182 bp in length, in which 18 251 sites (7.1%) were variable, 6110 sites (2.4%) were parsimony informative, with 8.9% missing data. After filtering the protein coding data further using posterior predictive checks, the 'filtered_data' dataset had a mean alignment length of 239 bp (range 74–524 bp), which resulted in a concatenated matrix 11 963 bp in length, of which 674 sites (5.6%) were variable, 599 sites (5%) were parsimony informative, with 7.8% missing data. The 'filtered_data' dataset consisted of datablocks selected from UCEs that were all unique, that is, none of the codon position datablocks were extracted from the same UCE. The dataset was biased toward the third codon position (66%, or 33 of 50 datablocks, see Supplementary Table S6).

The partitioning analysis of the 'full_data' dataset resulted in a 145-partition scheme (see Supplementary Table S4), whereas the analysis of the 'exon_data' dataset resulted in a 46-partition scheme. Model selection on the 'exon_data' dataset resulted in the assignment of 21 unique substitution models to the 46-partition scheme (see Supplementary Table S5). The resulting trees had strong overall support, with topologies diverging only within the outgroups or at shallow nodes in '*salvini* complex a' and '*aztecus* complex' (Fig. 3a).

Sequence processing and phylogenetic inference: mitochondria

I recovered complete mitochondrial genomes for 23 of the 25 specimens from UCE sequence reads, and partial genomes were constructed for the remaining two, with a mean coverage score of 147× (see Supplementary Table S2). Following annotation, 13 protein coding genes were identified and extracted. The

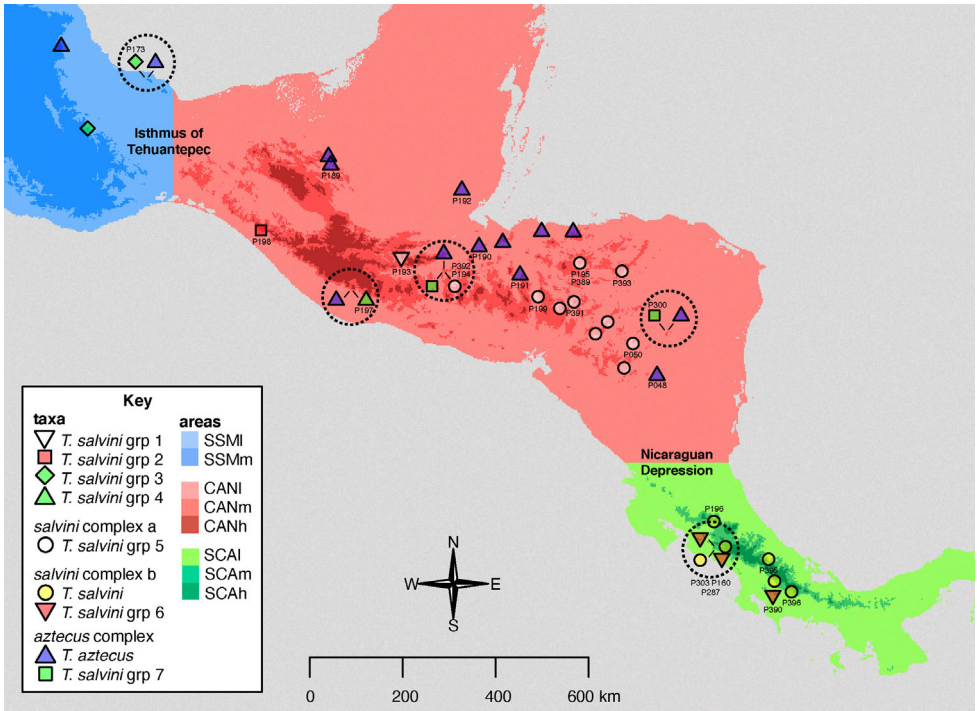

Fig 2. Distribution of the *Temnothorax salvini* group in Central America, showing the final species decisions inferred from this study. The major mountain complexes in Central America are colour coded and separated into the altitudinal zonation used in this study ($l < 1000$ m, $m = 1000–1800$ m and $h > 1800$ m). Dashed circles indicate places where species were collected in sympatry.. [Colour figure can be viewed at wileyonlinelibrary.com].

aligned, concatenated 'mt_data' matrix was 10 998 bp in length, of which 4241 sites (38.6%) were variable, with 1.2% missing data.

The model selection and partitioning analysis resulted in a seven-partition scheme, with six unique substitution models (see Supplementary Table S7). The resulting tree topology was nearly identical to the analyses of the 'full_data' and 'exon_data' datasets, differing in topology only in shallow, poorly supported parts of the phylogeny and with weaker support for several deeper nodes (Fig. 3b). Both analyses inferred three main complexes with broad geographic distributions and four more distantly related satellite morpho species, which is apparently more geographically restricted (compare Figs 2 and 3). Here, the three main complexes are referred to as: (i) the '*aztecus* complex', which occupies the SSM and extends southward across CAN to the Nicaraguan Depression, encompassing the type locality of *T. aztecus*, (ii) '*salvini* complex a', which spans the CAN from Guatemala to the Nicaraguan depression and (iii) '*salvini* complex b', which spans the SCA from Costa Rica to Panama, and encompasses the type locality of *T. salvini*.

Molecular species delimitation

The following results are summarized in Fig. 4a, b. I investigated DNA-based species delimitation and uncertainty using (i) the bPTP model, (ii) the STACEY model and (iii) the BPP model. In each case, specimens that had been diagnosed previously as *Temnothorax aztecus* and *T. salvini* were delimited into several species. In addition, a common finding among all of the following results is that samples from four populations across the SSM and CAN (P173, P193, P197 and P198) were each consistently delimited as individual species, leaving the three complexes mentioned above, which differed in delimitation scheme among analyses.

Two datasets were analysed with bPTP to generate species delimitation hypotheses: (i) 'bPTPnuc', which consists of the posterior distribution of trees from the ExaBayes analysis of the 'exon_data' dataset, and (ii) 'bPTPmit', which consists of posterior distribution of trees from the MrBayes tree generated from the analysis of the 'mt_data' dataset. The 'bPTPnuc' analysis presents a 12 species delimitation scheme, delimiting '*salvini* complex a' into a single species, while delimiting '*salvini* complex b' into a low-to-mid-elevation species and four mid-to-high elevation species; the '*aztecus* complex' was delimited into two species: one from mid-elevation in the CAN and a more widespread species from the low-to-mid elevations of the CAN and the SSM, which matches the morphology of the type material of *Temnothorax aztecus*. The 'bPTPmit' analysis delimited 16 species, splitting '*salvini* complex a' into a two species occupying the western and eastern CAN; compared to the 'bPTPnuc' analysis, the mid-to-low elevation specimens of '*salvini* complex b' were further divided into two species. In addition, the '*aztecus* complex' was delimited into four species: the mid-elevation species mentioned above, with the low-to-mid elevation populations delimited into three species.

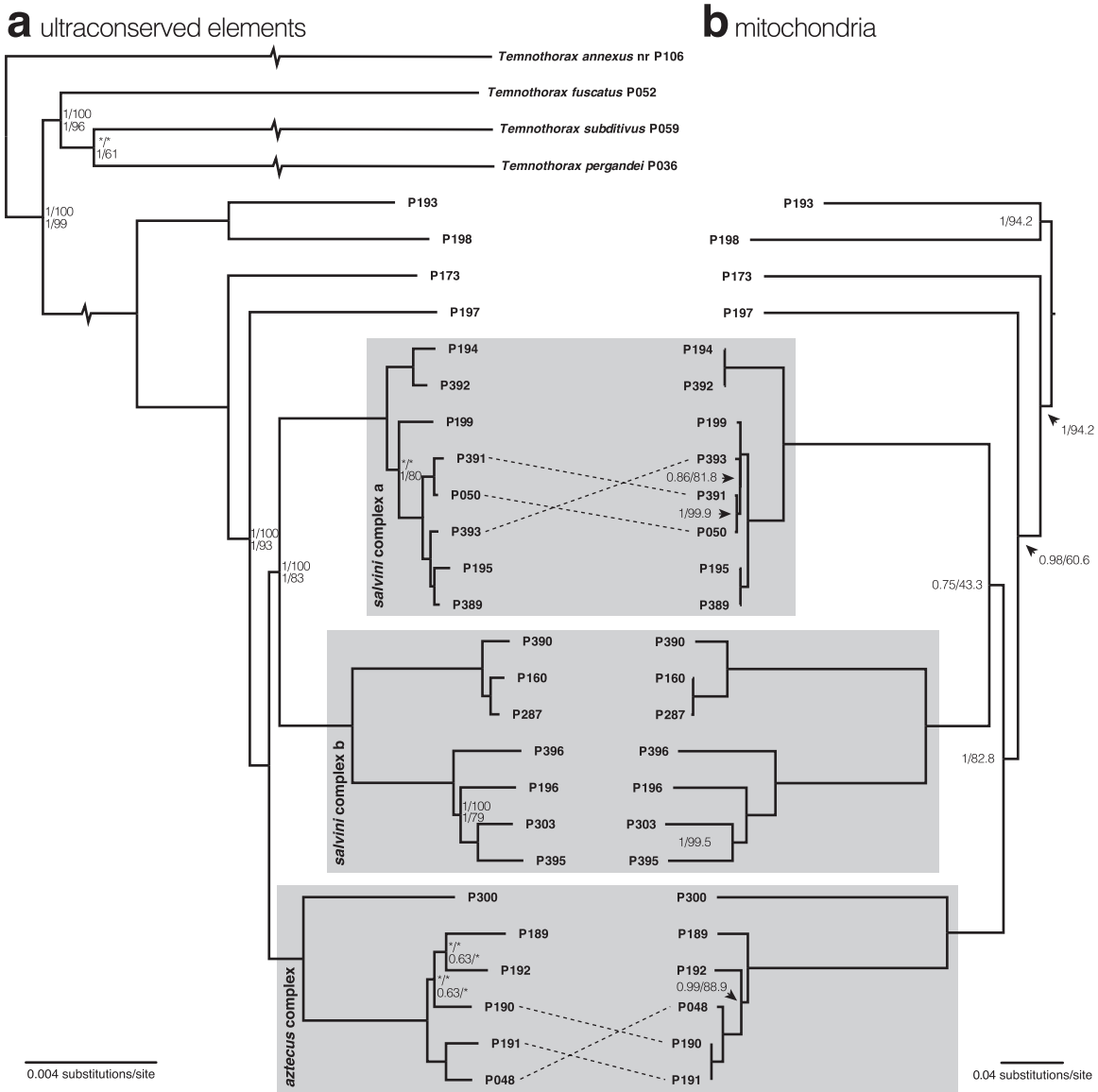

Fig 3. Phylogenies inferred from molecular data. Node support values for both trees are in posterior probability/ultrafast bootstrap, and only depicted when < 1/100. All taxon names of *salvini* group species are represented by extraction code only, and species complexes are indicated by shaded boxes. (a) Phylogeny based on the analysis of the 'exon_data' dataset with ExaBayes. Node values show support from analysis with ExaBayes and IQ-TREE2; support from analysis of the 'full_data' dataset is shown above, and the 'exon_data' values are below. (b) Phylogeny based on the analysis of the 'mt_data' dataset with MrBayes, depicting the node support values inferred from MrBayes and IQ-TREE2.

I ran two analyses in STACEY to generate species delimitation hypotheses: (i) 'STACEY nuc', consisting of the 'filtered_data' dataset and (ii) 'STACEY nuc + mit', consisting of the 'filtered_data_&_mt_data' dataset. Both analyses resulted in an overall topology that was nearly identical to the ExaBayes analysis of the 'exon_data' dataset, diverging only in the topology of one shallow clade (compare Figs 3a and 4a). The two analyses present delimitation hypotheses that differ in the number of species delimited: 'STACEY nuc' delimited eight species, grouping the specimens of the three complexes into four species, while 'STACEY nuc + mit' delimited the three complexes into ten species, further delimiting the specimens of '*salvini* complex b' into three species. Both analyses delimited the '*aztecus* complex' into two species, similar the 'bPTPnuc' analysis above.

I ran two analyses in BPP to generate species delimitation hypotheses: (i) 'BPP nuc', consisting of the 'filtered_data' dataset and (ii) 'BPP nuc + mit', consisting of the 'filtered_data_&_mt_data' dataset. The 'BPP nuc' analysis delimited ten species: like the 'bPTPmit' analysis, 'BPP nuc' split '*salvini* complex a' into two species, delimiting it into an eastern and western species, while '*salvini* complex b' was delimited into a low-to-mid elevation and a mid-to-high

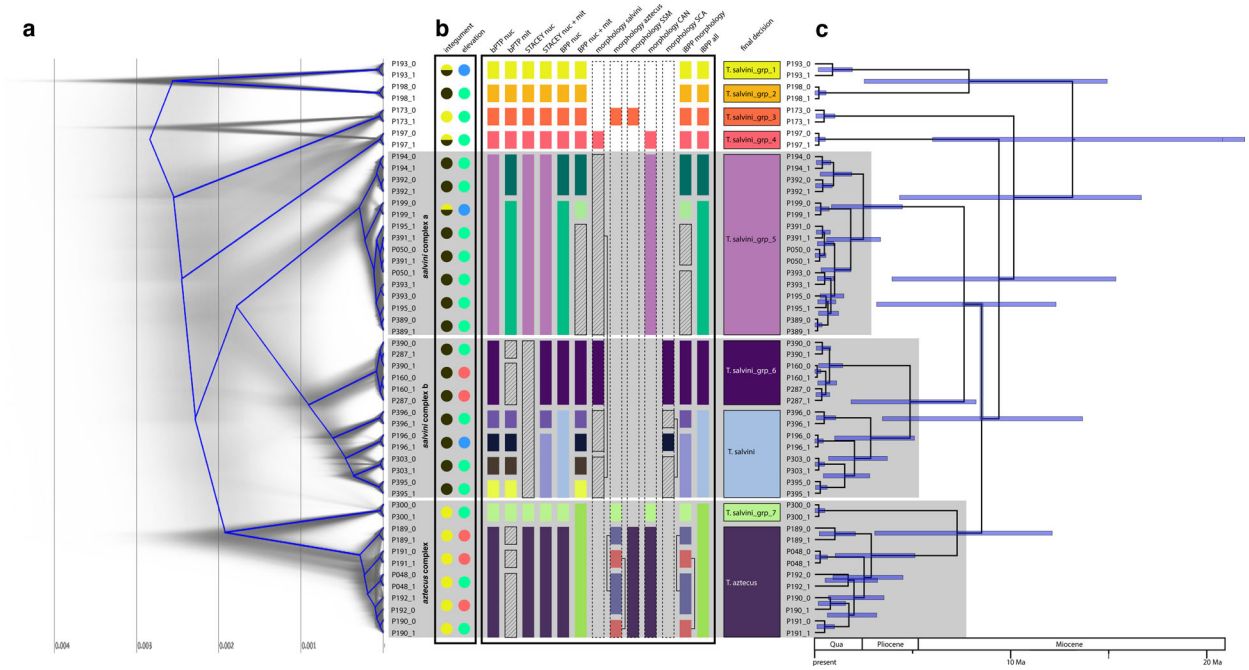

Fig 4. Species delimitation hypotheses and the evolutionary timescale of the *Temnothorax salvini* species group. (a) Cloudogram based on the analysis of the 'filtered_data' dataset with STACEY in grey, with the 'root canal' in blue, which summarizes the main features of the tree set (b) map of integument colour and elevation, and summary of species delimitation schemes from all analyses performed in this study. Solid coloured boxes in the species delimitation hypotheses denote a taxon delimited by more than one analysis, with each colour corresponding to a taxon hypothesis shared across more than one analysis. Hatched boxes denote hypotheses that delimited the taxon in only one analysis. (c) chronogram based on the analysis of the 'filtered_data' dataset with BEAST2. Error bars around nodes depict 95% highest posterior density.. [Colour figure can be viewed at wileyonlinelibrary.com].

elevation species; the '*aztecus* complex' was delimited into a mid-elevation and low-to-mid elevation species. The 'BPP nuc + mit' analysis, in contrast, delimited 13 species, further delimiting the western populations of '*salvini* complex a' into two species, one of which consists of a single high elevation population with bicolored integument; '*salvini* complex b' was delimited as in the 'bPTPnuc' analysis, recovering a low-to-mid elevation species, and each mid-to-high elevation population as distinct species; the '*aztecus* complex' was delimited as one species, irrespective of elevation.

Morphological validation

When the full morphometric dataset of 112 workers was analysed simultaneously, the clustering algorithm used in this study performed poorly, lumping all individuals into one cluster (results not shown). However, when subsets that included only morphologically similar or geographically co-distributed individuals were analysed, cluster analyses tended to converge on similar results as the molecular species delimitation approaches.

Specifically, the 'morphology *salvini*' data subset delimited the mid-to-low elevation specimens of '*salvini* complex b', but also delimited '*salvini* complex a' and a portion of the mid-to-high elevation '*salvini* complex b' specimens as a species, leaving the remainder of mid-to-high elevation '*salvini* complex b'; the latter two results are incongruent with the previous and following delimitation schemes. The 'morphology *aztecus*' data subset delimited specimens in a manner similar to the molecular delimitation analyses above, with the satellite population from southern Mexico delimited from the '*aztecus* complex', the remainder of which was delimited into mid and low elevation populations. However, this analysis further separated the mid-to-low elevation populations of the '*aztecus* complex' into eastern and western species. When only specimens from the CAN ('morphology CAN' in Fig. 4b) were analysed, the delimitation scheme was congruent with many of the molecular delimitation analyses, delimiting '*salvini* complex a' into one species and splitting the '*aztecus* complex' into high and low elevation species. The SSM analysis performed similarly ('morphology SSM' in Fig. 4b), with the mid-elevation population P300 delimited from the mid-to-low elevation populations of the larger '*aztecus* complex'. Morphological analysis of the SCA populations ('morphology SCA' in Fig. 4b) delimited the low-to-mid and mid-to-high elevation populations, but further delimited the high elevation populations into two species, in a manner incongruent with all other analyses in this study. The iBPP analysis of the 'morphology' dataset performed similarly to the 'BPP nuc + mit' analysis, but further delimited the eastern populations of '*salvini* complex a' into two species, delimited the Panamanian population from the rest of the mid-to-high elevation '*salvini* complex b' populations, and delimited the

low elevation '*aztecus* complex' populations into eastern and western species.

Total evidence species delimitation

The total-evidence analysis of the 'filtered_data_&_mt_data_morphology' dataset delimited ten species in a manner nearly identical to the 'BPP nuc' analysis but grouped all populations of the '*aztecus* complex' into one species (see Fig. 4b).

Delimitation scheme decision

Based on the decision rationale above, the final delimitation scheme had nine species. Specimens P193, P198, P173 and P197 were consistently found as separately delimited species among all analyses that included them. Delimitation schemes for '*salvini* complex a' differed among molecular methods and morphological methods; the specimens P194 and P392 were delimited in some molecular and morphological analyses, but these samples occur in the westernmost extreme of the distribution of the complex. Additionally, P199 was delimited from the remainder of '*salvini* complex a' in some analyses, but this sample was from a high elevation extreme of the distribution. All three specimens were lumped with the remainder of '*salvini* complex a' in the final scheme. Except for two molecular analyses, specimens P390, P160 and P287 were consistently delimited as a species in '*salvini* complex b'. The remaining four specimens had no consistent delimitation among analyses; all four species are represented by single, geographically distinct collections. It remains unclear if these represent a single, morphologically variable species; I conservatively lump them here as the previously described species *Temnothorax salvini*, but future collections may reveal that these are in fact distinct species with overlapping geographical ranges. Similarly, the molecular analyses differed in how the '*aztecus* complex' was delimited. However, specimen P300 was delimited in the morphological analyses and nearly all of the molecular analyses and is contained within the range of the remainder of the '*aztecus* complex'; I retain it as a species here. As for the '*aztecus* complex' exclusive of P300, there was some conflict between morphological analyses, but the more finely split delimitation scheme could be explained by geographical structure, with specimens P048 and P191 occupying the easternmost extreme of the species range. Because the samples of the '*aztecus* complex', exclusive of P300, are all allopatric, and P300 is sister to all of the remainder of the '*aztecus* complex' and sympatric with the more typical *T. aztecus*, I lump the '*aztecus* complex', exclusive of P300, into one previously described species, *Temnothorax aztecus*.

Divergence dating

Table 2 displays divergence dates of the species complexes and species inferred above; see Fig. 4c for a complete chronogram with age estimates and 95% highest posterior density intervals.

Table 2. Mean node ages and 95% highest posterior density intervals inferred from divergence dating analysis of the *Temnothorax salvini* group in BEAST2

Node	Mean	95% HPD
Crown *salvini* group	13.1	6.0–22.0
[*Temnothorax salvini* grp 1, *Temnothorax* salvini grp 2]	7.9	2.5–14.9
[*Temnothorax salvini* grp 3 [*Temnothorax* salvini grp 4 [aztecus complex [*Temnothorax* salvini grp 5, salvini complex b]]]]	10.2	4.3–16.7
[*Temnothorax salvini* grp 4 [aztecus complex [*Temnothorax* salvini grp 5, salvini complex b]]]	9.4	3.9–15.4
[*aztecus* complex [*Temnothorax salvini* grp 5, *salvini* complex b]]	8.5	3.4–13.7
[*Temnothorax salvini* grp 5, salvini complex b]	7.6	3.1–12.3
Temnothorax salvini grp 5	2.5	0.8–4.5
salvini complex b	4.8	1.8–8.2
aztecus complex	7.3	3.1–12.1
Temnothorax salvini grp 6	0.74	0.2–1.4
Temnothorax salvini	2.8	1.0–5.1
Temnothorax aztecus	2.9	1.0–5.1

Note: All ages are in millions of years ago.

The crown *salvini* group was estimated to have evolved 12.5 Ma ago, in the mid-Miocene, and much of the diversification that led to the present-day diversity within the *salvini* group occurred during the remainder of the Miocene. Although the crown ages for many singly sampled specimens remain undetermined, species containing multiple specimens in the final 9-species delimitation scheme ranged from 0.9 to 3.4 Ma ago.

Biogeography

I compared four scenarios of dispersal within the current range of the *salvini* group in Central America and compared the fit of the three models (DEC, DIVA-like and BayArea-like) within each scenario; see Table 3 for a comparison of results. The scenario with no dispersal to the SCA prior to 8 Ma ago, but without any dispersal constraint applied during the 5–8 Ma ago time period (scenario M3) was most highly supported, under the DIVA-like model (lnL −34.14; see Fig. 5 and Table 3), although this was only slightly better supported than the scenario with without any dispersal constraints (lnL −34.15; scenario M0 under the DIVA-like model; see Supplementary Figure S1). In both scenarios, the *salvini* group is estimated to have inhabited an ancestral range in the mid to high elevations of the CAN and the mid elevations of the SSM, which today remains the centre for the species diversity inferred in the present study. The two competing scenarios differ solely in how the ancestor of *T. salvini* grp 5, *T. salvini* grp 6 and *T. salvini* was inferred to have dispersed to the SCA: in M3, the ancestor of this clade dispersed to the high elevations of the CAN from the mid elevations, then expanded to the mid-elevations of the SCA, whereas in M0,

the ancestor dispersed to the mid-elevations of the SCA before expanding its range back into the high elevations of the CAN. In both scenarios, expansion and dispersal to low elevations in Central America only occurred in the Late Miocene, after 8 Ma ago. Overall, a pattern of early Miocene range contraction and Late Miocene range expansion can be applied to the results of the biogeographic analysis. In the Miocene-Pliocene transition, ranges appear to have contracted again (ancestors of *T. salvini* grp 1 and *T. salvini* grp 2; ancestors of *T. salvini* grp 5, *T. salvini* grp 6 and *T. salvini*). In addition, all taxa that inhabit multiple ranges in the present emerged in the Late Miocene and Pliocene.

Discussion

Congruence between species delimitation analyses

Molecular-based species delimitation approaches arrived at similar delimitation schemes regardless of whether UCE data or mitochondrial genome data were used, but the inclusion of mitochondrial data tended to lead to over-split delimitation schemes. Seven clusters within the *salvini* group were found consistently across all analyses: four geographically limited species, and three broadly distributed species complexes. Across all of the analyses, delimitation schemes conflicted exclusively in how the three widespread complexes were delimited. Possibly, these complexes inhabit a transitional space in the speciation continuum in which gene flow is becoming limited across broad geographic ranges and diverging ecological niches. Interestingly, the three most densely sampled species in the final delimitation scheme were all inferred to have crown ages of >2.5 Ma ago (see Table 2). Although comparative analyses of invertebrate species ages have not yet been performed, and may not yet be feasible for most groups, an age of 3 Ma ago bears a close resemblance to those found at the higher end of species ages in a broad analysis of vertebrate species (Cattin *et al.*, 2016). This observation may contribute to a growing body of evidence that the latitudinal diversity gradient in ants is a factor of lineage persistence (the "museum" hypothesis of Stebbins, 1974; Moreau & Bell, 2013) or niche conservatism (Losos, 2008; Economo *et al.*, 2018, 2019), and not speciation rate.

Biogeography

In this study, the *salvini* group was inferred to have originated in the mid-to-high elevations of the CAN and SSM approximately 13 Ma ago. A more coarsely scaled biogeographical analysis of the genus *Temnothorax* as a whole (Prebus, 2017) included only two specimens representing the *salvini* group, *T. aztecus* and a sample mistakenly identified as *T. salvini* (*T. salvini* grp 5 in this study). In Prebus (2017)the mean divergence date of *T. aztecus* and *T. salvini* grp 5 was approximately 11 Ma ago, which is older than the date inferred in the present study (8.5 Ma ago; see Table 2) but falls well within the range of 95% highest posterior density (13.7–3.4 Ma ago). In Prebus, 2017, the more inclusive *salvini* clade, which contains the *salvini* species group, was inferred to have had an extensive history of evolution in Central America, arriving in the Neotropics from a Nearctic ancestral range during the mid-Oligocene, with several lineages subsequently dispersing back to the Nearctic or the Greater Antilles throughout the Miocene. Corroborating the ancestral range found in this study, the *salvini* group was inferred to have had an ancestor with a Neotropical range. However, a major caveat is that the taxa of the *salvini* clade were not thoroughly sampled in Prebus (2017); if it is found, after more intensive sampling that the *salvini* clade has many early-diverging taxa with Nearctic ranges, the conclusion that the *salvini* clade is primarily Neotropical may shift.

The inference that the mid-to-high elevations of Central America were especially important during the early evolution of the *salvini* group may reflect the climatic trends during the mid to late Miocene, when global temperatures began to drop ca. 14 Ma ago after the mid Miocene climatic optimum (Zachos *et al.*, 2001; Hansen *et al.*, 2013). Dispersal of the presumably cold-adapted *salvini* group to the SCA from the CAN may have occurred as habitats associated with mid to high elevations in Central America expanded, in tandem with mountain building in present day Costa Rica and Panama. Branstetter & Longino (2019) found a similar pattern in *Ponera* ants, suggesting that periodic expansion and contraction of mesic forest during the Plio-Pleistocene may have led to a grade of cryptic species, which originated in the Nearctic and successively penetrated further into Central America in concert with cycles of global climate change.

Within the *salvini* group, only two members appear west of the Isthmus of Tehuantepec, a savannah-like depression between the CAN and the SSM: *T. aztecus* and the undescribed lookalike species *T. salvini* grp 3. The former is found at the low to mid elevations of the Los Tuxtlas volcano complex and the SSM in Mexico, while the latter inhabits solely mid elevations in these same localities. *T. salvini* grp 3 was inferred to have been isolated in the SSM following a range contraction in the Late Miocene ~10 Ma ago, with *T. aztecus* arriving later following its more recent expansion throughout low and mid elevations of Central America from an initial dispersal to lowland habitats in the late Miocene ~7 Ma ago.

In this study, three broadly distributed species complexes were inferred: *Temnothorax aztecus* was found to be widespread in the low-to-mid elevations of Central America north of the Nicaraguan depression, whereas *T. salvini* inhabits the mid-to-high elevations of the SCA, and *T. salvini* grp 5 occupies a large range in the mid-to-high elevations in the CAN. An unexpected result of this study was that many members of the *salvini* group appear to occupy moderately overlapping elevational niches within each mountain complex, with mid-to-high elevation species apparently having small geographical ranges. These observations raise the possibility that the *salvini* group is involved in a taxon cycle dynamic between its members (Wilson, 1959; Wilson, 1961; Ricklefs & Bermingham, 2002; Economo *et al.*, 2015). In its classical sense, the taxon cycle is a process inferred to explain the distributions of species across island archipelagos. The process involves sequential range expansions and contractions, which leads to a present-day pattern in which to lineages that arrive on islands early are

Table 3. Biogeographic scenarios compared in the BioGeoBEARs analysis

Scenario	Dispersal between SCA and rest of range > 5 Ma ago	SCA allowed > 8 Ma ago	LnL		
			DEC	DIVALIKE	BAYAREALIKE
M0	1	1	−35.23	−34.15	−34.84
M1	0.01	1	−35.13	−36.33	−35.29
M2	0.01	0	−37.26	−36.81	−36.94
M3	1	0	−35.46	**−34.14**	−35.59

Note: SCA, southern Central American cordilleras. Resulting LnL of the highest scoring model is shown in bold.

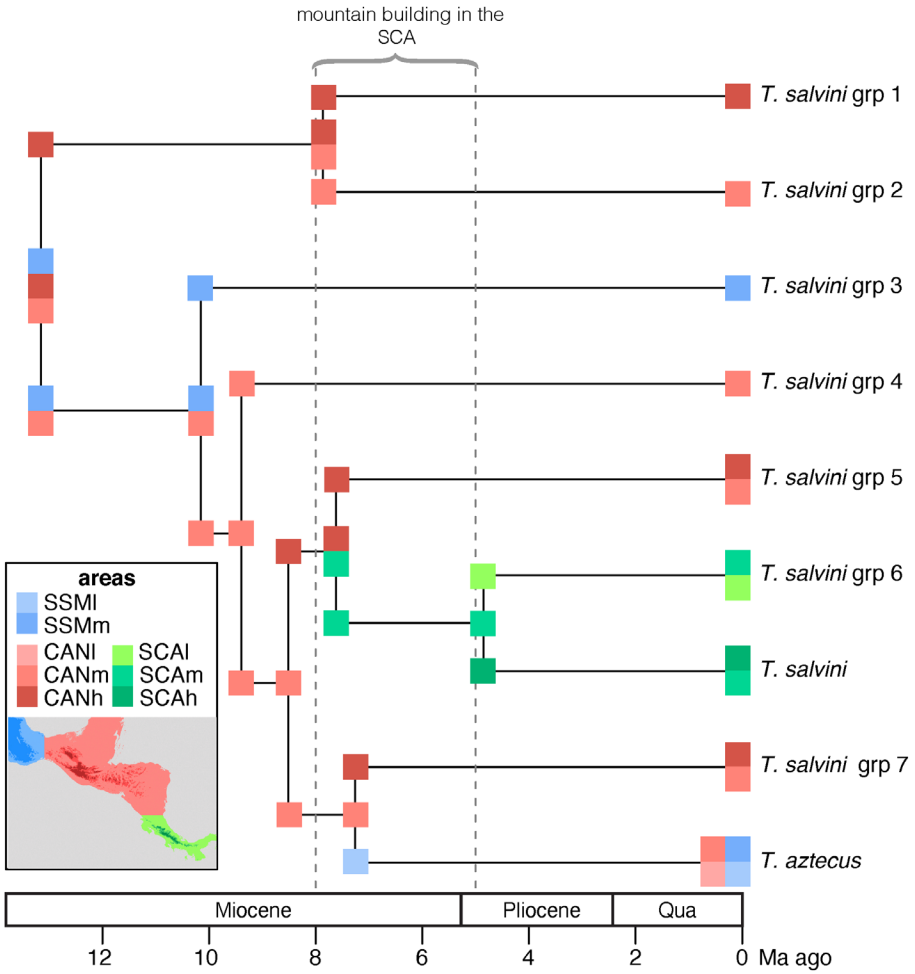

Fig 5. Historical biogeography of the *Temnothorax salvini* group inferred from the chronogram output from BEAST2 and current species ranges, using the programme BioGeoBEARS. The major mountain complexes in Central America are colour coded and separated into the altitudinal zonation used in this study ($l < 1000$ m, $m = 1000–1800$ m, and $h > 1800$ m). The output of the model and scenario with the highest likelihood is shown: DIVA-like on scenario M3.. [Colour figure can be viewed at wileyonlinelibrary.com].

represented by species with reduced ranges, often in interior island habitats (via range contraction), and species with large ranges, sometimes spanning several islands, are found mainly marginal island habitats (via recent range expansion). However, in this case, the mid-to-high elevations of Central America stand in for the interior island habitats of the classical scenario, and the lowlands are the marginal island habitats. In this scenario, *T. aztecus* represents the most recent expansion phase into marginal habitats, and *T. salvini* and *T. salvini* grp 6 are newly established taxon in the SCA.

Delimitation of populations versus species

High throughput sequencing methods present a vast leap in the amount of data that can be used to infer species limits,

Fig 6. Images of *Temnothorax salvini* group worker specimens of species recognized in this study, in profile view. Scale bars represent 0.2 mm. Unique specimen identifiers follow the taxon name (a) *Temnothorax* salvini_grp_3, CASENT0758791, (b) *Temnothorax aztecus*, CASENT0758793, (c) *Temnothorax* salvini_grp_5, CASENT0758892, (d) *Temnothorax* salvini_grp_2, JTLC000010282, (e) *Temnothorax* salvini_grp_1, CASENT0614495, (f) *Temnothorax* salvini_grp_7, CASENT0629030, (g) *Temnothorax salvini*, CASENT0756074, (h) *Temnothorax* salvini_grp_6, CASENT0758334, (i) *Temnothorax* salvini_grp_4, CASENT0756087.. [Colour figure can be viewed at wileyonlinelibrary.com].

but many of the current methods are still only feasible with comparatively small molecular datasets. In this study, I chose to filter a UCE dataset down to a size that is compatible with many of the current methods, including those based on the multispecies coalescent. Species delimitation methods based on the multispecies coalescent have recently been criticized for delimiting populations instead of species in cases where the metapopulation shows high geographical structure (Sukumaran & Knowles, 2017; Chambers & Hillis, 2020). Several of the analyses presented in the current study indicated the same tendency, with populations at the geographical extremes of the species range being delimited as species (see Fig. 4 and the Results section above). However, my approach mitigated this issue by comparing multiple different delimitation methods, independently analysing morphological data to validate species delimitation hypotheses, and by incorporating geographical range data to demonstrate sympatry and allopatry among MOTUs. While not used in the current study, the development of methods capable of using large molecular datasets to infer species delimitation is underway, which show great promise for their applicability to complex problems (Fujisawa *et al.*, 2016; Derkarabetian *et al.*, 2019). In the case of MOTUs with non-overlapping geographic ranges, however, the issue of whether the units being detected with such methods are highly structured metapopulations or allopatric species still looms, especially if these analyses are conducted without an integrative framework and in the absence of information about gene flow.

Conclusion

Until the present study, the *salvini* species group contained two named species: *Temnothorax salvini* and *T. aztecus*. Despite their morphological similarities (see Fig.6b, g), these two putative species were easily distinguished from each other by the colour of their integument. The preceding study finds that the *salvini* group is much more diverse than previously thought. To generate a candidate set of delimitation hypotheses, I used a combination of species tree estimation, molecular species delimitation methods and morphometric validation. To mitigate the possibility that the delimitation schemes were reflecting population structure instead of reproductive isolation, the candidate delimitation hypotheses were viewed through the lens of present-day geographic distributions, finding that

many of the species inferred in the delimitation analyses have overlapping ranges. Taken together, these pieces of evidence suggest that the units being detected are often sympatric and not exchanging genes, and therefore, most likely represent independently evolving species. The results suggest that an additional seven species are contained within this group, all of which are morphologically distinguishable from each other *a posteriori*. Descriptions of the new species of the *Temnothorax salvini* group will be included in a future comprehensive taxonomic revision of the larger, more inclusive *salvini* clade.

Supporting Information

Additional supporting information may be found online in the Supporting Information section at the end of the article.

Fig. S1. Full set of output figures from all scenarios and models tested in the BioGeoBEARs analysis. M = Southern Sierra Madres, N = Central American Nucleus, C = southern Central American cordilleras; $l < 1000$ m, $m = 1000–1800$ m, and $h > 1800$ m.

Table S1. List of specimens used in this study. Specimens extracted for molecular analysis are indicated by their extraction codes.

Table S2. List of specimens used for molecular analyses with associated barcode adapters, UCE and mitochondrial genome assembly summary statistics.

Table S3. NCBI accession numbers of specimens and molecular datasets used in the study.

Table S4. Characteristics of the partitions of the 'full_data' dataset inferred by PartitionFinder2.

Table S5. Characteristics of the partitions of the 'exon_data' dataset inferred by PartitionFinder2, with substitution models selected by IQ-TREE2.

Table S6. Characteristics of the datablocks comprising the 'filtered_data' dataset.

Table S7. Partitions and substitution models identified by IQ-TREE2 for a maximum likelihood analysis of the 'mt_data' dataset.

Acknowledgements

Many of the specimens used in this study came from the projects ALAS, LLAMA and ADMAC, which are the products of a vast number of contributors, but which have been managed by Robert Colwell, John Longino, Robert Anderson, Philip Ward and Michael Branstetter. I wish to thank Brian Fisher of the California Academy of Sciences, and Brian Brown of the Natural History Museum of Los Angeles Entomology Collection for facilitating museum loans of additional specimens for this study, and Christian Rabeling, Brendon Boudinot, Philip Ward, Steven Messer, Kyle Gray, Laura Daniela Mera Rodriguez and two anonymous reviewers for providing invaluable comments and feedback on earlier versions of the manuscript. This work was supported by National Science Foundation grant DEB-1354996 (Project ADMAC), awarded to Philip Ward.

The author declares no conflict of interest.

Data availability

All new raw Illumina reads generated for this study have been deposited at the NCBI Sequence Read Archive (SRA), BioProject PRJNA669896; the Illumina reads of several samples (*Temnothorax annexus*nr P106, *Temnothorax fuscatus* P052, *Temnothorax subditivus* P059 and *Temnothorax pergandei* P036) were from a previously published study, and can be found on the NCBI SRA, BioProject PRJNA393044. All mitochondrial genome sequences generated in this project have been deposited at GenBank (accession numbers MW233593–MW233617). A complete table of NCBI accession numbers, assembly statistics and associated barcode adapters for all specimens used in this study can be found in Supplementary Table S3. All UCE and mitochondrial matrices used in this study, all Trinity contigs, all UCE contigs, all tree files, all data analysis input files and all custom scripts used in this study have been deposited at the Dryad Digital Repository (https://doi.org/10.25338/B8V33D).

References

Abascal, F., Zardoya, R. & Telford, M.J. (2010) TranslatorX: multiple alignment of nucleotide sequences guided by amino acid translations. *Nucleic Acids Research*, **38**, 7–13.

Aberer, A.J., Kobert, K. & Stamatakis, A. (2014) ExaBayes: massively parallel Bayesian tree inference for the whole-genome era. *Molecular Biology and Evolution*, **31**, 2553–2556.

Adams, M., Raadik, T.A., Burridge, C.P. & Georges, A. (2014) Global biodiversity assessment and hyper-cryptic species complexes: more than one species of elephant in the room? *Systematic Biology*, **63**, 518–533.

Allio, R., Schomaker-Bastos, A., Romiguier, J., Prosdocimi, F., Nabholz, B. & Delsuc, F. (2020) MitoFinder: efficient automated large-scale extraction of mitogenomic data in target enrichment phylogenomics. *Molecular Ecology Resources*, **00**, 1–14.

Andermann, T., Fernandes, A.M., Olsson, U. *et al.* (2019) Allele phasing greatly improves the phylogenetic utility of ultraconserved elements. *Systematic Biology*, **68**, 32–46. https://doi.org/10.1093/sysbio/syy039.

Bacon, C.D., Silvestro, D., Jaramillo, C., Smith, B.T., Chakrabarty, P. & Antonelli, A. (2015) Biological evidence supports an early and complex emergence of the Isthmus of Panama. *Proceedings of the National Academy of Sciences*, **112**, 6110–6115.

Baird, N.A., Etter, P.D., Atwood, T.S. *et al.* (2008) Rapid SNP discovery and genetic mapping using sequenced RAD markers. *PLoS One*, **3**, e3376.

BaroniUrbani, C. (1978) Materiali per una revisione dei *Leptothorax* neotropicali appartenenti al sottogenere *Macromischa* Roger, n. Comb. (Hymenoptera: Formicidae). *Ent Basiliensia*, **3**, 395–618.

Barraclough, T.G. (2019) *The evolutionary biology of species*. Oxford, UK: *Oxford University Press*.

Bauer, A.M., Parham, J.F., Brown, R.M. *et al.* (2011) Availability of new Bayesian-delimited gecko names and the importance of character-based species descriptions. *Proceedings of the Royal Society B: Biological Sciences*, **278**, 490–492.

Baur, H. & Leuenberger, C. (2011) Analysis of ratios in multivariate morphometry. *Systematic Biology*, **60**, 813–825.

Bercovitch, F.B., Berry, P.S., Dagg, A. *et al.* (2017) How many species of giraffe are there? *Current Biology*, **27**, R136–R137.

Bernt, M., Donath, A., Jühling, F. *et al.* (2013) MITOS: improved de novo metazoan mitochondrial genome annotation. *Molecular Phylogenetics and Evolution*, **69**, 313–319.

Bi, K., Vanderpool, D., Singhal, S., Linderoth, T., Moritz, C. & Good, J.M. (2012) Transcriptome-based exon capture enables highly cost-effective comparative genomic data collection at moderate evolutionary scales. *BMC Genomics*, **13**, 403.

Bolger, A.M., Lohse, M. & Usadel, B. (2014) Trimmomatic: A flexible trimmer for Illumina sequence data. *Bioinformatics*, btu170. **30**, 2114–2120.

Bollback, J.P. (2002) Bayesian model adequacy and choice in phylogenetics. *Molecular Biology and Evolution*, **19**, 1171–1180.

Borowiec, M.L. (2016) AMAS: a fast tool for alignment manipulation and computing of summary statistics. *PeerJ*, **4**, e1660.

Borowiec, M.L. (2019) Convergent evolution of the army ant syndrome and congruence in big-data phylogenetics. *Systematic Biology*, **68**, 642–656. https://doi.org/10.1093/sysbio/syy088.

Bouckaert, R., Vaughan, T.G., Barido-Sottani, J. *et al.* (2019) BEAST 2.5: An advanced software platform for Bayesian evolutionary analysis. *PLoS Computational Biology*, **15**, e1006650.

Branstetter, M.G. & Longino, J.T. (2019) Ultra-conserved element phylogenomics of new world *Ponera* (Hymenoptera: Formicidae) illuminates the origin and phylogeographic history of the endemic exotic ant *Ponera exotica*. *Insect Systematics and Diversity*, **3**, 1–13. https://doi.org/10.1093/isd/ixz001.

Branstetter, M.G., Longino, J.T., Ward, P.S. & Faircloth, B.C. (2017) Enriching the ant tree of life: enhanced UCE bait set for genome-scale phylogenetics of ants and other Hymenoptera. *Methods in Ecology and Evolution*, **8**, 768–776.

Brown, J.M., Hedtke, S.M., Lemmon, A.R. & Lemmon, E.M. (2010) When trees grow too long: investigating the causes of highly inaccurate Bayesian branch-length estimates. *Systematic Biology*, **59**, 145–161.

Burbrink, F.T., Yao, H., Ingrasci, M., Bryson, R.W. Jr, Guiher, T.J. & Ruane, S. (2011) Speciation at the Mogollon Rim in the Arizona mountain kingsnake (*Lampropeltis pyromelana*). *Molecular Phylogenetics and Evolution*, **60**, 445–454.

Carstens, B.C., Pelletier, T.A., Reid, N.M. & Satler, J.D. (2013) How to fail at species delimitation. *Molecular Ecology*, **22**, 4369–4383.

Castresana, J. (2000) Selection of conserved blocks from multiple alignments for their use in phylogenetic analysis. *Molecular Biology and Evolution*, **17**, 540–552.

Cattin, L., Schuerch, J., Salamin, N. & Dubey, S. (2016) Why are some species older than others? A large-scale study of vertebrates. *BMC Evolutionary Biology*, **16**, 90.

Chambers, E.A. & Hillis, D.M. (2020) The multispecies coalescent over-splits species in the case of geographically widespread taxa. *Systematic Biology*, **69**, 184–193 https://doi.org/10.1093/sysbio/syz042.

Clegg, M.T., Gaut, B.S., Learn, G.H. & Morton, B.R. (1994) Rates and patterns of chloroplast DNA evolution. *Proceedings of the National Academy of Sciences*, **91**, 6795–6801.

Creighton, W.S. (1950) The ants of North America. *Bulletin of the Museum of Comparative Zoology at Harvard College*, **104**, 1–585.

Csősz, S. & Fisher, B.L. (2015) Diagnostic survey of Malagasy *Nesomyrmex* species-groups and revision of *hafahafa* group species via morphology based cluster delimitation protocol. *ZooKeys*, **526**, 19.

Denyer, P. & Kussmaul, S. (2012) *Geología de Costa Rica*. Cartago, Costa Rica: *Instituto Tecnológico de Costa Rica*.

Derkarabetian, S., Castillo, S., Koo, P.K., Ovchinnikov, S. & Hedin, M. (2019) A demonstration of unsupervised machine learning in species delimitation. *Molecular Phylogenetics and Evolution*, **139**, 106562. https://doi.org/10.1016/j.ympev.2019.106562.

Dierckxsens, N., Mardulyn, P. & Smits, G. (2016) NOVOPlasty: De novo assembly of organelle genomes from whole genome data. *Nucleic Acids Research*, **45**, e18. https://doi.org/10.1093/nar/gkw955.

Domingos, F.M., Bosque, R.J., Cassimiro, J., Colli, G.R., Rodrigues, M.T., Santos, M.G. & Beheregaray, L.B. (2014) Out of the deep: cryptic speciation in a Neotropical gecko (Squamata, Phyllodactylidae) revealed by species delimitation methods. *Molecular Phylogenetics and Evolution*, **80**, 113–124.

Duque-Caro, H. (1990) Neogene stratigraphy, paleoceanography and paleobiogeography in northwest South America and the evolution of the Panama Seaway. *Palaeogeography, Palaeoclimatology, Palaeoecology*, **77**, 203–234.

Economo, E.P., Sarnat, E.M., Janda, M. *et al.* (2015) Breaking out of biogeographical modules: range expansion and taxon cycles in the hyperdiverse ant genus *Pheidole*. *Journal of Biogeography*, **42**, 2289–2301.

Economo, E.P., Narula, N., Friedman, N.R., Weiser, M.D. & Guénard, B. (2018) Macroecology and macroevolution of the latitudinal diversity gradient in ants. *Nature Communications*, **9**, 1–8.

Economo, E.P., Huang, J.P., Fischer, G. *et al.* (2019) Evolution of the latitudinal diversity gradient in the hyperdiverse ant genus *Pheidole*. *Global Ecology and Biogeography*, **28**, 456–470.

Faircloth, B.C. (2016) PHYLUCE is a software package for the analysis of conserved genomic loci. *Bioinformatics*, **32**, 786–788.

Faircloth, B.C., McCormack, J.E., Crawford, N.G., Harvey, M.G., Brumfield, R.T. & Glenn, T.C. (2012) Ultraconserved elements anchor thousands of genetic markers spanning multiple evolutionary timescales. *Systematic Biology*, **61**, 717–726.

Faircloth, B.C., Branstetter, M.G., White, N.D. & Brady, S.G. (2015) Target enrichment of ultraconserved elements from arthropods provides a genomic perspective on relationships among Hymenoptera. *Molecular Ecology Resources*, **15**, 489–501.

Fennessy, J., Bidon, T., Reuss, F. *et al.* (2016) Multi-locus analyses reveal four giraffe species instead of one. *Current Biology*, **26**, 2543–2549.

Fujisawa, T., Aswad, A., Barraclough, T.G. (2016) A rapid and scalable method for multilocus species delimitation using bayesian model comparison and rooted triplets. *Systematic Biology*, **65**, 759–771. http://dx.doi.org/10.1093/sysbio/syw028.

Grabherr, M.G., Haas, B.J., Yassour, M. *et al.* (2011) Full-length transcriptome assembly from RNA-seq data without a reference genome. *Nature Biotechnology*, **29**, 644–652.

Gueuning, M., Frey, J.E. & Praz, C. (2020) Ultraconserved yet informative for species delimitation: UCEs resolve long-standing systematic enigma in Central European bees. *Molecular Ecology*, **29**, 4203–4220. https://doi.org/10.1111/mec.15629.

Haddrill, P.R., Charlesworth, B., Halligan, D.L. & Andolfatto, P. (2005) Patterns of intron sequence evolution in Drosophila are dependent upon length and GC content. *Genome Biology*, **6**, R67.

Hahn, C., Bachmann, L. & Chevreux, B. (2013) Reconstructing mitochondrial genomes directly from genomic next-generation sequencing reads – a baiting and iterative mapping approach. *Nucleic Acids Research*, **41**, e129–e129.

Hansen, J., Sato, M., Russell, G. & Kharecha, P. (2013) Climate sensitivity, sea level and atmospheric carbon dioxide. *Philosophical Transactions of the Royal Society A: Mathematical, Physical and Engineering Sciences*, **371**, 20120294.

Hoang, D.T., Chernomor, O., Von Haeseler, A., Minh, B.Q. & Vinh, L.S. (2018) UFBoot2: improving the ultrafast bootstrap approximation. *Molecular Biology and Evolution*, **35**, 518–522.

Höhna, S., Landis, M.J., Heath, T.A. *et al.* (2016) RevBayes: Bayesian phylogenetic inference using graphical models and an interactive model-specification language. *Systematic Biology*, **6**, 726–736.

Huelsenbeck, J.P. & Ronquist, F. (2001) MRBAYES: Bayesian inference of phylogeny. *Bioinformatics*, **17**, 754–755.

Hughes, A.L. & Yeager, M. (1997) Comparative evolutionary rates of introns and exons in murine rodents. *Journal of molecular evolution*, **45**, 125–130.

Iturralde-Vinent, M. & MacPhee, R.D. (1999) Paleogeography of the Caribbean region: implications for Cenozoic biogeography. *Bulletin of the AMNH*, **238**, 1–95.

Ješovnik, A., Sosa-Calvo, J., Lloyd, M.W., Branstetter, M.G., Fernandez, F. & SchultzT, R. (2017) Phylogenomic species delimitation and host-symbiont coevolution in the fungus-farming ant genus *Sericomyrmex* Mayr (Hymenoptera: Formicidae): ultraconserved elements (UCEs) resolve a recent radiation. *Systematic Entomology*, **42**, 523–542.

Jones, G. (2017) Algorithmic improvements to species delimitation and phylogeny estimation under the multispecies coalescent. *Journal of Mathematical Biology*, **74**, 447–467.

Kalyaanamoorthy, S., Minh, B.Q., Wong, T.K., von Haeseler, A. & Jermiin, L.S. (2017) ModelFinder: fast model selection for accurate phylogenetic estimates. *Nature Methods*, **14**, 587.

Katoh, K. & Standley, D.M. (2013) MAFFT multiple sequence alignment software version 7: improvements in performance and usability. *Molecular Biology and Evolution*, **30**, 772–780.

Kelchner, S.A. (2002) Group II introns as phylogenetic tools: structure, function, and evolutionary constraints. *American Journal of Botany*, **89**, 1651–1669.

Kirby, S.H. (2007) Geological processes and orchid biogeography with applications to southeast Central America. *Lankesteriana International Journal on Orchidology*, **7**, 53–55.

Lanfear, R., Calcott, B., Kainer, D., Mayer, C. & Stamatakis, A. (2014) Selecting optimal partitioning schemes for phylogenomic datasets. *BMC Evolutionary Biology*, **14**, 82.

Lanfear, R., Frandsen, P.B., Wright, A.M., Senfeld, T. & Calcott, B. (2016) PartitionFinder 2: new methods for selecting partitioned models of evolution for molecular and morphological phylogenetic analyses. *Molecular Biology and Evolution*, msw260. **34**, 772–773.

Larsson, A. (2014) AliView: a fast and lightweight alignment viewer and editor for large data sets. *Bioinformatics*, **30**, 3276–3278.

Leaché, A.D. & Fujita, M.K. (2010) Bayesian species delimitation in West African forest geckos (*Hemidactylus fasciatus*). *Proceedings of the Royal Society B: Biological Sciences*, **277**, 3071–3077.

Learn, G.H. Jr, Shore, J.S., Furnier, G.R., Zurawski, G. & Clegg, M.T. (1992) Constraints on the evolution of plastid introns: the group II intron in the gene encoding tRNA-Val (UAC). *Molecular Biology and Evolution*, **9**, 856–871.

Lemmon, A.R., Emme, S.A. & Lemmon, E.M. (2012) Anchored hybrid enrichment for massively high-throughput phylogenomics. *Systematic Biology*, **61**, 727–744.

Li, H. (2013) Aligning sequence reads, clone sequences and assembly contigs with BWA-MEM. *arXiv preprint*, **1303**, 3997.

Longino, J.T. & Branstetter, M.G. (2020) Phylogenomic species delimitation, taxonomy, and 'Bird Guide' identification for the neotropical Ant genus *Rasopone* (Hymenoptera: Formicidae). *Insect Systematics and Diversity*, **4**, 1.

Losos, J.B. (2008) Phylogenetic niche conservatism, phylogenetic signal and the relationship between phylogenetic relatedness and ecological similarity among species. *Ecology Letters*, **11**, 995–1003.

MacKay, W.P. (1993) The status of the ant *Leptothoraxpergandei* Emery (Hymenoptera: Formicidae). *Sociobiology*, **21**, 287.

Masonick, P. & Weirauch, C. (2020) Integrative species delimitation in Nearctic ambush bugs (Heteroptera: Reduviidae: Phymatinae): insights from molecules, geometric morphometrics and ecological associations. *Systematic Entomology*, **45**, 205–223.

Matzke, N.J. (2013) Probabilistic historical biogeography: new models for founder-event speciation, imperfect detection, and fossils allow improved accuracy and model-testing. *Frontiers of Biogeography*, **5**, 242–248.

Mayr, E. (1942) *Systematics and the origin of species*. Columbia University Press, New York.

McCole, R.B., Erceg, J., Saylor, W. & Wu, C.T. (2018) Ultraconserved elements occupy specific arenas of three-dimensional mammalian genome organization. *Cell Reports*, **24**, 479–488.

Milne, I., Stephen, G., Bayer, M. *et al.* (2013) Using Tablet for visual exploration of second-generation sequencing data. *Briefings in Bioinformatics*, **14**, 193–202.

Moreau, C.S. & Bell, C.D. (2013) Testing the museum versus cradle tropical biological diversity hypothesis: phylogeny, diversification, and ancestral biogeographic range evolution of the ants. *Evolution*, **67**, 2240–2257.

Nguyen, L.T., Schmidt, H.A., Von Haeseler, A. & Minh, B.Q. (2015) IQ-TREE: a fast and effective stochastic algorithm for estimating maximum-likelihood phylogenies. *Molecular Biology and Evolution*, **32**, 268–274.

Nurk, S., Meleshko, D., Korobeynikov, A. & Pevzner, P.A. (2017) metaSPAdes: a new versatile metagenomic assembler. *Genome Research*, **27**, 824–834.

Pie, M.R., Bornschein, M.R., Ribeiro, L.F., Faircloth, B.C. & McCormack, J.E. (2019) Phylogenomic species delimitation in microendemic frogs of the Brazilian Atlantic Forest. *Molecular Phylogenetics and Evolution*, **141**, 106627.

Prebus, M. (2017) Insights into the evolution, biogeography and natural history of the acorn ants, genus *Temnothorax* Mayr (hymenoptera: Formicidae). *BMC Evolutionary Biology*, **17**, 250.

R Core Team (2019) *R: A language and environment for statistical computing*. R Foundation for Statistical Computing, Vienna, Austria. https://www.R-project.org/.

Rannala, B. & Yang, Z. (2003) Bayes estimation of species divergence times and ancestral population sizes using DNA sequences from multiple loci. *Genetics*, **164**, 1645–1656.

Ree, R.H. & Sanmartín, I. (2018) Conceptual and statistical problems with the DEC+J model of founder-event speciation and its comparison with DEC via model selection. *Journal of Biogeography*, **45**, 741–749. https://doi.org/10.1111/jbi.13173.

Ricklefs, R.E. & Bermingham, E. (2002) The concept of the taxon cycle in biogeography. *Global Ecology and Biogeography*, **11**, 353–361.

Ritchie, A.M., Lo, N. & Ho, S.Y.W. (2017) The impact of the tree prior on molecular dating of data sets containing a mixture of inter- and intraspecies sampling. *Systematic Biology*, **66**, 413–425.

Rohland, N. & Reich, D. (2012) Cost-effective, high-throughput DNA sequencing libraries for multiplexed target capture. *Genome Research*, **22**, 939–946.

Ronquist, F. & Huelsenbeck, J.P. (2003) MRBAYES 3: Bayesian phylogenetic inference under mixed models. *Bioinformatics*, **19**, 1572–1574.

Scrucca, L., Fop, M., Murphy, T.B. & Raftery, A.E. (2016) Mclust 5: clustering, classification and density estimation using Gaussian finite mixture models. *The R Journal*, **8**, 205–233.

Seifert, B. & Csösz, S. (2015) *Temnothorax crasecundus* sp. n. – a cryptic Eurocaucasian ant species (Hymenoptera, Formicidae) discovered by Nest Centroid Clustering. *ZooKeys*, **479**, 37–64. https://doi.org/10.3897/zookeys.479.8510.

Sistrom, M., Donnellan, S.C. & Hutchinson, M.N. (2013) Delimiting species in recent radiations with low levels of morphological divergence: a case study in Australian *Gehyra* geckos. *Molecular Phylogenetics and Evolution*, **68**, 135–143.

Solís-Lemus, C., Knowles, L.L. & Ané, C. (2015) Bayesian species delimitation combining multiple genes and traits in a unified framework. *Evolution*, **69**, 492–507. https://doi.org/10.1111/evo.12582.

Stamatakis, A. (2014) RaxML version 8: a tool for phylogenetic analysis and post-analysis of large phylogenies. *Bioinformatics*, **30**, 1312–1313.

Stebbins, G.L. (1974) *Flowering plants: evolution above the species level*. Cambridge, US: *Harvard University Press*.

Subramanian, S. & Kumar, S. (2003) Neutral substitutions occur at a faster rate in exons than in noncoding DNA in primate genomes. *Genome research*, **13**, 838–844.

Sukumaran, J. & Knowles, L.L. (2017) Multispecies coalescent delimits structure, not species. *Proceedings of the National Academy of Sciences U.S.A.*, **114**, 1607–1612.

Sullivan, J. & Swofford, D.L. (2001) Should we use model-based methods for phylogenetic inference when we know that assumptions about among-site rate variation and nucleotide substitution pattern are violated? *Systematic Biology*, **50**, 723–729.

Tagliacollo, V.A. & Lanfear, R. (2018) Estimating improved partitioning schemes for ultraconserved elements. *Molecular Biology and Evolution*, **35**, 1798–1811.

Takahata, N., Satta, Y. & Klein, J. (1995) Divergence time and population size in the lineage leading to modern humans. *Theoretical Population Biology*, **48**, 198–221.

Tirosh, I., Bilu, Y. & Barkai, N. (2007) Comparative biology: beyond sequence analysis. *Current Opinion in Biotechnology*, **18**, 371–377.

Wilson, E.O. (1959) Adaptive shift and dispersal in a tropical ant fauna. *Evolution*, **13**, 122–144.

Wilson, E.O. (1961) The nature of the taxon cycle in the Melanesian ant fauna. *The American Naturalist*, **95**, 169–193.

Yang, Z. (2006) *Computational molecular evolution*, p. 376. *Oxford University Press*, Oxford.

Yang, Z. (2015) The BPP program for species tree estimation and species delimitation. *Current Zoology*, **61**, 854–865. https://doi.org/10.1093/czoolo/61.5.854.

Zachos, J., Pagani, M., Sloan, L., Thomas, E. & Billups, K. (2001) Trends, rhythms, and aberrations in global climate 65 Ma to present. *Science*, **292**, 686–693.

Zhang, J., Kapli, P., Pavlidis, P. & Stamatakis, A. (2013) A general species delimitation method with applications to phylogenetic placements. *Bioinformatics*, **29**, 2869–2876.

Accepted 19 November 2020